Univerzita Karlova v Praze
Matematicko-fyzikální fakulta

DIPLOMOVÁ PRÁCE

Jiří Prchal

Experimentální studium elektronových vlastností systému $RT_{1-x}T'_xAl$

Katedra fyziky elektronových struktur

Vedoucí diplomové práce: Mgr. Pavel Javorský, Dr.

Studijní program: Fyzika kondenzovaných a makromolekulárních látek

In this place, I would like to say my best thanks to everyone, who supported me to raise this work and helped me in the whole study anyway.

First of all, I wish to express my gratitude to my supervisor Mgr. Pavel Javorský, Dr. for his solicitous and patient leading me for all time of this work, support during many experiments, for many important information, for his conscientious care about my understanding to all problems I needed to, and for productive discussions while formatting, and collaboration while correcting this work.

I am also grateful to Prof. RNDr. Vladimír Sechovský, DrSc. for his disinterested care about my work and studies and inspiration into the area of magnetic studies.

I owe my thanks to everybody, who introduced me to many interesting experimental techniques and working with the instruments.

I would like to thank to Jana Vejpravová and RNDr. Pavel Svoboda, CSc. for their assistance when preparing the samples.

My thanks belong to Mgr. Milan Dopita and Doc. RNDr. David Rafaja, CSc. for their help with x-ray analysis and executing lattice parameters.

I wish to express another thanks to Mgr. Karel Jurek, CSc. for performance of the microprobe expriment.

I am thankful to RNDr. Eva Šantavá, CSc. and ing. Josef Šebek, ing. Miroslav Maryško, CSc. and Mgr. Aleksandr Kolomiyets, Dr. for their care about my magnetization measurements.

My gratitude belongs to my family, especially to my mother for her every-day care, understanding and support.

Prohlašuji, že jsem svou diplomovou práci napsal samostatně a výhradně s použitím citovaných pramenů. Souhlasím se zapůjčováním práce.

V Praze dne 19.dubna 2002 Jiří Prchal

Contents

Abstrakt:

Název práce: **Experimentální studium elektronových vlastností systému $RT_{1-x}T'_xAl$**
Autor: Jiří Prchal
Katedra: Katedra fyziky elektronových struktur
Vedoucí diplomové práce: Mgr. Pavel Javorský, Dr.
e-mail vedoucího: javor@mag.mff.cuni.cz

Abstrakt:

Sloučeniny *R*NiAl a *R*CuAl patří ke skupině sloučenin typu *RTX* (*R* ~ vzácná zemina, *T* ~ tranzitivní kov, *X* ~ *p*-prvek), které krystalizují v hexagonální struktuře typu ZrNiAl (prostorová grupa P-62m). Zajímavé vlastnosti byly pozorovány u série $TbNi_{1-x}Cu_xAl$ vzhledem k změně mechanismu zodpovědného za magnetické uspořádání. Přechod od ErNiAl k ErCuAl navíc zahrnuje změnu krystalové anizotropie.

ErNiAl je antiferomagnet (AF) s momenty uspořádanými v bazální rovině, ErCuAl je feromagnet (F) s momenty podél osy *c*. $ErNi_{1-x}Cu_xAl$ vykazuje ‚skok' mřížových parametrů mezi $x = 0.5$ a 0.6 v teplotách do 5 K. Podle měření magnetizace a měrné tepelné kapacity se uspořádání z AF do F děje mezi $x = 0.2$ a $x = 0.4$. V oblasti $0.05 \leq x \leq 0.20$ je možná koexistence F a AF složek, vzorky v tomto oboru vykazují dva fázové přechody, což pro $x = 0.05$ potvrdila i měření tepelné kapacity. Vzorky s $x \geq 0.4$ vykazují ferromagnetické chování.

Konečné rozhodnutí o uspořádání erbiových momentů vyžaduje změření neutronové difrakce.

Klíčová slova: intermetalika vzácných zemin, magnetizace, měrná tepelná kapacita, magnetické uspořádání.

Abstract:

Title: **Experimental study of the electronic properties of the $RT_{1-x}T'_xAl$ system**
Author: Jiří Prchal
Department: Department of Electronic Structures
Supervisor: Mgr. Pavel Javorský, Dr.
Supervisor's e-mail address: javor@mag.mff.cuni.cz

Abstract:

The *R*NiAl and *R*CuAl compounds belong to a large group of *RTX* compounds (*R* ~ rare-earth, *T* ~ transition metal, *X* ~ *p*-metal) crystallizing in the ZrNiAl-type hexagonal structure, space group P-62m (group No.189). Very interesting behaviour has been observed for $TbNi_{1-x}Cu_xAl$ system, what has been attributed to a change of mechanisms responsible for the magnetic ordering. In comparison to it, $ErNi_{1-x}Cu_xAl$ series represent a more complex system. Change of magnetocrystalline anizotropy between the boundary stoichiometric concentrations is involved additionally.

ErNiAl is an antiferromagnet (AF) with magnetic moments aligned within the basal plane below 6.2 K, ErCuAl is a simple ferromagnet (F) with moments aligned along the *c*-axis below 6.8 K. While increasing parameter *x*, a dramatic 'jump' of lattice constants occurs between $x = 0.5$ and 0.6 in temperatures down to 5 K. The magnetization and heat capacity data indicate that the change from AF to F ordering occurs between $x = 0.2$ and $x = 0.4$. In the range $0.05 \leq x \leq 0.20$ there is possible the coexistence of F and AF alignment, the samples in this region embody two phase transitions. This was for $x = 0.05$ confirmed by heat capacity measurements. The samples with $x \geq 0.4$ exhibit ferromagnetic behaviour.

The neutron diffraction measurements are desired for the final decision about the details of the ordering of Er-moments in the studied series.

Keywords: rare-earth intermetallics, magnetization, heat capacity, magnetic ordering

1. Introduction

During last years, interest on the compounds containing elements with partly filled electronic *f*-shell is increasing because of their physical properties. Especially magnetic behaviour caused by the unfilled *f*-shell is being studied. The main difference between 4*f* and 5*f* electrons relates to their character - the 4*f* electrons are well localized, but the 5*f* ones exhibit more itinerant behaviour.

The ternary compounds represent a higher number of structure types, on the other hand they exhibit a larger base of compounds from which more compounds crystallize in the same structure type. So the rare-earth ions can be studied in various types of crystalline environment. When substituting elements, one changes the number of electrons in the system gradually. Consequent adding *d*-electrons into the sample, by substituting of the transition metal by the neighbouring one, can lead to the change in type of magnetic ordering, which is in rare-earths mediated mainly by the electrons in the conduction band, i.e. by the *s* and *d* ones.

This work is focused on the magnetic behaviour of the $ErNi_{1-x}Cu_xAl$ pseudo-ternary series, where Cu is being substituted instead of Ni, and its comparison to the crystal structure. It belongs to a large group of *RTX* (*R* ~ rare-earth, *T* ~ transition metal, *X* ~ *p*-metal) compounds crystallizing in the hexagonal ZrNiAl-type structure. The motivation to deal just by this series origins in previous studies of the *R*NiAl and *R*CuAl compounds [1,2] at the Department of Electronic Structures of the Charles University and interesting results obtained for similar $TbNi_{1-x}Cu_xAl$ compounds by Ehlers et al. [3]. The boundary compounds of the Tb-based series exhibit different type of magnetic ordering while that of the Er-based series in addition embody difference in the orientation of magnetic moments. Thus it was expected more complex behaviour than $TbNi_xCu_{1-x}Al$ showed.

During this work, samples of chosen values of the parameter *x* have been prepared, attested and studied by means of x-rays, magnetization and several of them by heat capacity experiments to obtain information about the crystal structure and the bulk magnetic properties.

2. Theory

Rare earth ions

The set of elements placed between lanthanum (Z = 57) and lutetium (Z = 71) in the Periodic Table of Elements are called 'lanthanides' and together with scandium (Z = 21) and yttrium (Z = 39) create group called 'Rare-earths' (for historical reasons). The elements from lanthanum to europium (Z = 63) are usually marked as 'light rare-earths' and the other (i.e. Gd to Lu) are 'heavy rare-earths'. In further text we will mark them all as '*R*'.

It is known, that the atomic radius of rare-earths decreases with increasing atomic number. It is so called lanthanide-contraction. The electronic configuration of these elements can be generally written as:

$$[\mathrm{Xe}]\ 6s^2 5d^1 4f^N. \tag{2.1}$$

Just the 4*f* electrons are responsible for the magnetic momenta. Thus the magnetic behaviour of rare-earths origins in consequent filling of the electronic 4*f*-shell.

Because the energy of 5*d* electrons is higher than that of 4*f*, rare-earths are mostly found in the trivalent state. In solids, the 5*d* and 6*s* electrons are delocalised and create the conduction band.

The 4*f*-shell has much lower (about ten times) radial extent (≈ 40 pm) then the typical distance between the neighbouring rare-earth atoms in solid. It is also shielded by the full 5*s*- and 5*p*-shells. Then the character of 4*f* electrons is rather localised unlike to that of 5*f* electrons which exhibit all types of behaviour between localised and itinerant. That is why one can consider rare-earth atoms in solid to be free ions placed in a sea of conduction electrons with *s*, *d* and *p* character. The 4*f* level of such ion is not directly influenced by the neighbouring atoms and behaviour of it's electrons depends on their interaction with the charge of nucleus shielded by the inner filled electron shells and with another 4*f* electrons. The effect of other filled shells can be included together with the nuclear charge in a central potential of an effecive charge of $+\widetilde{Z}e$. When neglecting the spin-orbit interaction the total Hamiltonian of such system is given by

$$\hat{H}_{4f} = \sum_{i=1}^{N}\left(-\frac{\hbar^2}{2m_e}\right)\nabla_i^2 + \sum_{i=1}^{N}-\frac{\widetilde{Z}e^2}{\boldsymbol{r}_i} + \sum_{i<j}\frac{e^2}{\boldsymbol{r}_{ij}}\ . \tag{2.2}$$

Here, $\hbar$, m_e and e are the Planck's constant, static weight and charge of electron, respectively. The variables $\boldsymbol{r}_i$ and $\boldsymbol{r}_{ij}$ are the positions of the electron in relation to the central potential and electrons between each other. Because the interelectronic distances are highly correlated, we can use, for classifying the energy levels, the Hartree-Fock approximation:

$$\hat{H}_0 = \sum_{i=1}^{N}\left(-\frac{\hbar^2}{2m_e}\right)\nabla_i^2 + \sum_{i=1}^{N}-\frac{\tilde{Z}e^2}{\boldsymbol{r}_i} + \sum_{i=1}^{N}V_i(\boldsymbol{r}) \ , \qquad (2.3)$$

where $V_i(\boldsymbol{r})$ are the Hartree-Fock self-consistent potentials.

The electron states are characterized by the hydrogen-like wave functions

$$\psi_{nlm_lm_s}(\boldsymbol{r},\sigma) = R_{nl}(r)\cdot Y_{m_l}(\vartheta,\varphi)\cdot\chi_{m_s}(\sigma) \ , \qquad (2.4)$$

where $R_{nl}(r)$, $Y_{m_l}(\vartheta,\varphi)$ and $\chi_{m_s}(\sigma)$ are the radial, spherical and spin wave functions, respectivelly, and n, l, m_l, m_s are the basic, orbital, magnetic and spin quantum numbers.

The ground state corresponding to the $4f^N$ electron configuration can be determined by the assignment of N electrons to the $4f$ one electron states ($n = 4$, $l = 3$). The total wave function can be represented by a Slater determinant of N one-electron wave functions. The ground state is generally degenerated with the degeneracy of $\binom{14}{N}$. This degeneracy is partly removed by the correlation and spin-orbit interactions.

The correlation interaction is given by:

$$\hat{H}_{corr} = \sum_{i<j}\frac{e^2}{r_{ij}} - \sum_{i=1}^{N}V_i(\boldsymbol{r}) \ . \qquad (2.5)$$

Because it is much smaller than the interaction given by $\hat{H}_0$, it can be computed as the perturbation of the Hamiltonian (2.3). This interaction is the origin of splitting of the states into so-called terms, which are characterized by the orbital ($\boldsymbol{L} = \sum \boldsymbol{l}_i$) and spin momenta ($\boldsymbol{S} = \sum \boldsymbol{s}_i$). The operators $\hat{\boldsymbol{L}}^2$, $\hat{\boldsymbol{S}}^2$, $\hat{\boldsymbol{L}}_z$ and $\hat{\boldsymbol{S}}_z$ commute with $\hat{H}_{corr}$, so the stationary states are given by the values L, S, M_L and M_S. The energy levels do not depend on M_L and M_S and they stay $(2L+1)(2S+1)$-fold degenerated according

to the values of M_L and M_S. The ground term is defined by following the Hund's rules [4]:

1. S reaches the maximum while maintaining the Pauli exclusion principle.
2. L has the maximum value in accordance with the first rule.

The spin-orbit interaction origins from the relativistic correlation of the electron spin and its own orbital momenta. In our case (rare earth intermetallic) it is much weaker than the correlation interaction and can be included as a perturbation. According to the Russel-Saunders approximation the Hamiltonian of spin-orbit interaction can be taken as a coupling between $\hat{\boldsymbol{L}}$ and $\hat{\boldsymbol{S}}$:

$$\hat{H}_{LS} = \lambda(LS)\cdot\hat{\boldsymbol{L}}\hat{\boldsymbol{S}} \ , \tag{2.6}$$

where λ is the effective spin-orbit constant. This spin-orbit interaction leads to the splitting of spectral terms into so-called multiplets according to the total angular momentum $J = L+S$. Each multiplet remains $(2J+1)$-fold degenerated. The ground multiplet can be determined from the third Hund's rule: $J = |L - S|$ for the rare earths with the 4f-shell filled from less than half ($N < 7$), $J = L + S$ for the heavy-rare earths ($N \geq 7$). The magnetic moment and spin of the ground multiplet are given by $\boldsymbol{\mu} = -\mu_B g_J \boldsymbol{J}$ and $\boldsymbol{S} = (g_J - 1)\boldsymbol{J}$, where g_J is the Landé factor:

$$g_J = 1 + \frac{J(J+1)+S(S+1)-L(L+1)}{2J(J+1)} \ . \tag{2.7}$$

Crystal field

In crystal, the surrounding ions and electrons product a field which act on the rare-earth ion. This field is called crystal field and it keeps the symmetry of the crystal lattice. In the case of rare-earths the 4f-moments are well shielded by the full 5s- and 5d-shells and the "4f electrons — crystal field" interaction can be considered as a perturbation. This perturbation leads to a complete or a partial remove of the degeneracy of the ground multiplet.

Using the point-charge model the first approximation of the crystal-field Hamiltonian $\hat{H}_{CF}$ can be simply computed. The surrounding electric charges product the electrostatic potential, which can be at a point $\boldsymbol{r} = (r, \theta, \varphi)$ expressed as:

$$V_{CF}(\boldsymbol{r}) = \sum_j \frac{q_j}{|\boldsymbol{R}_j - \boldsymbol{r}|} , \tag{2.8}$$

where q_j is a charge at the position $\boldsymbol{R}_j$ of an ion. If a charge q_i is at $\boldsymbol{r}_i$, then the crystal-field Hamiltonian is given by:

$$\hat{H}_{CF} = \sum_i q_i V_{CF}^i = \sum_{i,j} \frac{q_i q_j}{|\boldsymbol{R}_j - \boldsymbol{r}_i|} , \tag{2.9}$$

where i runs over all 4f electrons in the unfilled shell.

To determine the energy levels and the eigenfunctions of the rare-earth ion in the crystal field, we have to calculate the matrix elements of perturbing Hamiltonian between free-ion states. The crystal-field Hamiltonian can be expressed as:

$$\hat{H}_{CF} = \sum_{n,m} B_n^m \hat{O}_n^m . \tag{2.10}$$

Here, B_n^m and $\hat{O}_n^m$ are the crystal-field parameters and crystal-field operators, respectively [5].

According to the Kramers theorem [6] the energy levels of ions, that have an odd number of electrons (4f-electrons for the rare-earths), are at least twofold and evenly degenerated. Another work [7] showed, that the ions with even number of electrons tend to have a singlet energy levels in crystals due to the lowered symmetry, what completely removes the degeneracy of the energy levels.

There are several methods to study the crystal field. The most effective one is the inelastic neutron scattering. Thermal neutrons with the energy of the same order as the energy splitting due to crystal field, scattered inelastically on the magnetic ion, can induce a transition between two crystal-field levels of this ion. Also specific heat measurements are usefull for study of crystal-field spectra, especially in cases of well separated energy levels. Additional information can be obtained from susceptibility and magnetization measurements, but to obtain indispensable information, single crystal experiments are necessary.

Exchange interactions

Ordering of magnetic moments has its origin in exchange interactions. Generally, in solids there are two basic types of exchange interactions: the direct exchange and weak indirect interaction including the indirect RKKY interaction (see *Fig. 2.1*).

In rare-earth-based compounds the direct overlap of the 4*f*-electronic wave functions is negligible. Therefore the direct interaction (typical for 3*d*-metals) cannot be usually considered as responsible for magnetic ordering in these materials. Instead, the indirect interactions should be taken into account.

There are various types of indirect interaction. The conduction electrons mediate the weak RKKY interaction. These electrons are spin polarized because of the presence of magnetic moment in the surroundings. Owing to properties of conduction electrons this type of interaction is long range and is oscillating according the distance from the original magnetic ion. The polarized electrons then interact with the neighbouring magnetic moments. This type of interaction has the basic importance in ordering of magnetic moments of well-localized electrons and is mostly found in lanthanides and their compounds.

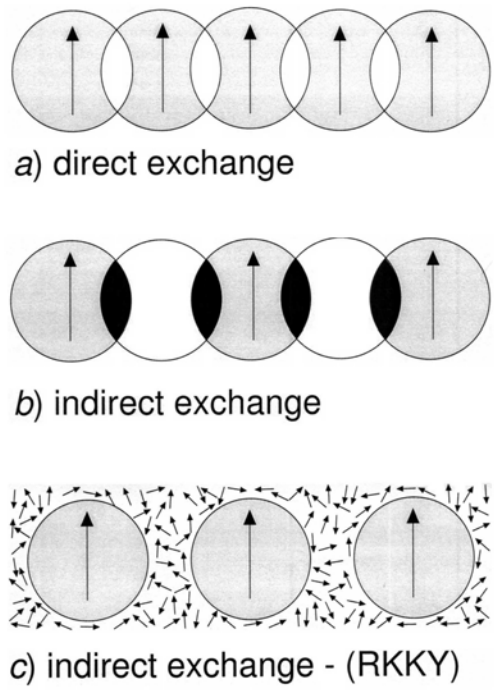

Fig. 2.1: *The two basic types of exchange interactions, including the indirect RKKY interaction [8].*

In the Heisenberg model, the exchange interaction energy between two ions can be expressed as:

$$\hat{H}_{ij\_ex} = -2J_{ij}\hat{\boldsymbol{S}}_i\hat{\boldsymbol{S}}_j \ , \tag{2.11}$$

where J_{ij} is the exchange integral between the spins $\hat{\boldsymbol{S}}_i$ and $\hat{\boldsymbol{S}}_j$. The total Hamiltonian for the whole system is then:

$$\hat{H}_{ex} = -\sum_{\substack{i,j \\ i\neq j}} J_{ij}\hat{\boldsymbol{S}}_i\hat{\boldsymbol{S}}_j \ . \tag{2.12}$$

In case of exchange coupling between 4*f*-moments, we shall mention two mechanisms of indirect exchange. The first one considers the RKKY interaction mediated by conduction electrons. The Hamiltonian of this interaction is:

$$\hat{H}_{\mathrm{RKKY}} = -\tfrac{1}{2}\sum_{i,j} \mathrm{J}(\boldsymbol{R}_i\text{-}\boldsymbol{R}_j)\boldsymbol{J}_i\boldsymbol{J}_j \ , \tag{2.13}$$

where we sum over all rare-earth ions with the momenta $\boldsymbol{J}_i$, $\mathrm{J}(\boldsymbol{R}_i\text{-}\boldsymbol{R}_j)$ is the effective exchange parameter. Corresponding critical temperature T_{C} and the paramagnetic Curie temperature θ_{p} are proportional to the de-Gennes factor $(g_{\mathrm{J}}\text{-}1)^2 J(J+1)$.

The second description was proposed by Campbell [9]. It supposes the coupling between 4*f*-moments to be mediated by the 5*d* rare-earth electrons. In consequence of *f*-*d* exchange coupling a positive local *d*-moment is induced. Because the 5*d* electrons of the rare-earth are more delocalised and the wave functions can overlap, one can consider direct exchange interaction, which favours in this case ferromagnetic coupling, and positive value of Curie paramagnetic temperature is expected. Furthermore, in compounds with transition metals, the exchange between rare-earth 5*d*-states and *d*-states of the transition metal has to be considered.

3. Previous results

3.1 RTX compounds

Crystal Structure

RTX form a relatively large group of compounds consisted from rare-earth (*R*), transition metal (*T*) and *p*-metal (metal with unfilled *p*-shell of electrons, from the IIIB, IVB or VB group of the Periodic Table) (*X*) elements.

The *RTX* compounds crystallize in various structures. The most usual are three types: orthorhombic TiNiSi-type structure, hexagonal AlB_2-type structure and hexagonal ZrNiAl-type structure.

Most compounds from the *R*NiAl, *R*CuAl, *R*PdAl, *R*NiIn, *R*CuIn, *R*PdIn, *R*AuIn, *R*RhSn and *R*PdTl series crystallize in the ZrNiAl-type hexagonal structure [10]. Generally, in this crystal structure type crystallize more heavy- than light rare-earth based compounds. There are several *RTX* compounds (e.g. TbPtSn [11]), crystallizing in the ZrNiAl-type or in the orthorhombic TiNiSi-type structure, depending on the way of preparation.

Magnetic properties

From the view of magnetic properties, the *RTX* compounds crystallizing in the ZrNiAl-type structure have not been studied so systematically and the interest on these compounds is increasing. Quite complex study on the basis of magnetization, susceptibility, specific heat, electrical resistivity and also neutron diffraction, was performed for the *R*NiAl and *R*CuAl series [2,1] (see below). Just several of the other *RTX* compounds have been studied. An antiferromagnetic (AF) behaviour was observed e.g. for some *R*RhSn [12], *R*PtSn [13], *R*AgGe [14] compounds. For some of e.g. *R*ptIn [15], *R*pdAl [16] and for DyAgGe [14] ferromagnetic (F) behaviour has been reported.

Some anomalous magnetic behaviour has been observed for Ce- and Yb-based compounds. For instance CePdIn [17], CePdAl [18] and YbNiAl [19,20] were found to be antiferromagnetically ordered with heavy-fermion behaviour, CePtIn is a nonmagnetic heavy-fermion system [21], CeNiIn is a valence-fluctuating system with a Kondo-like behaviour [22].

*3.2 R*NiAl *and R*CuAl

The crystal structure of the *R*NiAl and *R*CuAl series was first described by Dwight et al. in 1968 [23]. Except for the La-based materials, all the *R*NiAl and *R*CuAl compounds crystallize in the ZrNiAl-type hexagonal structure (space group $P\bar{6}2m$). We describe this structure in details in the chapter *5.1.1*.

Magnetic properties of the *R*NiAl and *R*CuAl compounds have been studied relatively thoroughly within past years, especially by Oesterreicher [24], Tuan [2] and Javorský [1].

In early seventies of the twentieth century there were made deductions about all of these compounds to be subtle ferromagnets, except for CeNiAl which remains paramagnetic down to the temperature of 4.2 K and for ErNiAl and TmNiAl which were found to behave metamagnetically [24].

Later, in 1992, another results of the magnetic properties of *R*NiAl compounds were published [2]. The new measurements showed compounds with the heavy rare-earths (i.e. Gd-Tm) to undergo two or three magnetic phase transitions. Compounds with R = Gd, Tb, Dy, Ho show coexistence of ferro- and antiferromagnetic interactions. The magnetic ordering temperature in the *R*NiAl series is roughly proportional to de-Gennes factor. The exception is PrNiAl where enhanced ordering temperature was ascribed to a stronger hybridization between 4*f* and ligand states. An intermediate valence state of Ce ions was speculated in CeNiAl. The coexistence of ferro- and antiferromagnetic ordering in *R*NiAl for R = Tb, Dy and Ho has been confirmed by neutron diffraction experiments [25,26]. Incommensurate magnetic structures have been found in PrNiAl and NdNiAl [27]. *Figure 3.1* shows the dependence of the ordering temperature of the *R* element in *R*NiAl series.

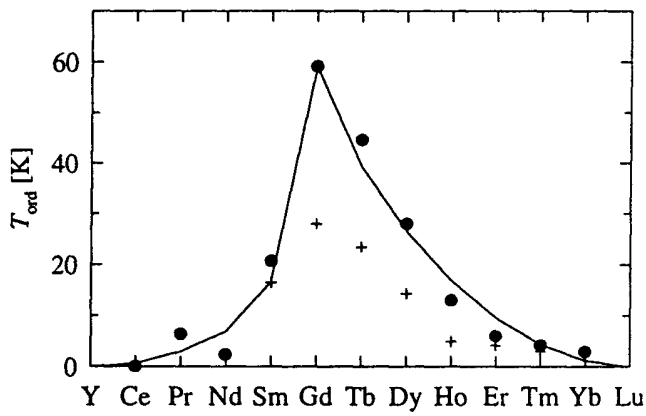

***Fig. 3.1**: Dependences of the ordering temperatures T_{ord} (circles) and additional magnetic phase transition temperatures (cross) on the rare-earth (R) element in the RNiAl compounds [2,1].*

The study of magnetic properties in *R*CuAl series is given in Refs. [28,1]. YCuAl and LuCuAl exhibit a Pauli paramagnetic behaviour. The heavy rare-earth *R*CuAl compounds have been found as ferromagnets except for indications of antiferromagnetic ordering observed in low-temperature phase of DyCuAl. No magnetic ordering in TmCuAl was reported in [28], while an AF order below 1.9K was reported in [29]. Complex AF order at low temperatures was confirmed recently by neutron diffraction [30]. Among the light rare-earths, PrCuAl behaves antiferromagnetically and coexistence of ferro- and antiferromagnetic ordering has been observed. *Figure 3.2* shows the dependence of the ordering temperature of the *R* element in *R*CuAl series.

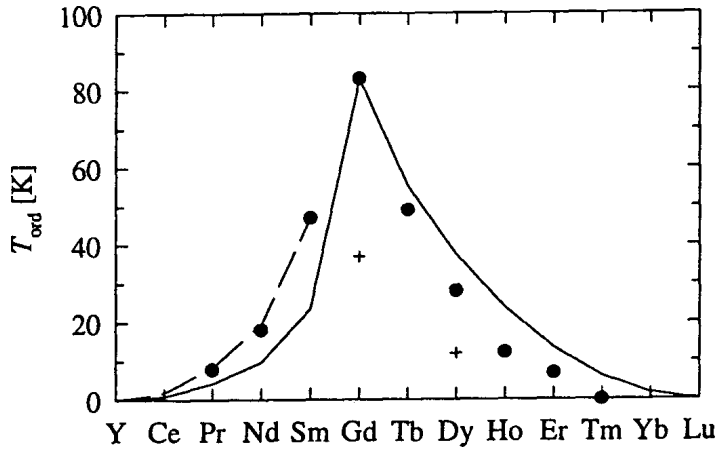

***Fig. 3.2**: Dependences of the ordering temperatures T_{ord} (circles) and additional magnetic phase transition temperatures (cross) on the rare-earth (R) element in the RCuAl compounds [1].*

3.3 ErNiAl and ErCuAl, $TbNi_{1-x}Cu_xAl$

ErNiAl and ErCuAl

As follows from that written above, ErNiAl and ErCuAl both crystallize in the ZrNiAl-type structure. The ErNiAl compound has been found to be antiferromagnet and ErCuAl ferromagnet. Both these compounds have been studied by powder neutron difffraction, specific heat, magnetization and susceptibility measurements [2,31].

The ErNiAl compound orders antiferromagnetically below $T_N = 6.2$ K. The Er moments lie within the basal plane and create a 'triangle' structure as shown in *Fig. 3.3*. This magnetic structure is described by the propagation vector $\boldsymbol{k} = (1/2,0,1/2)$. The magnitude of the Er moments reaches 6.8 μ_B at 1.8 K.

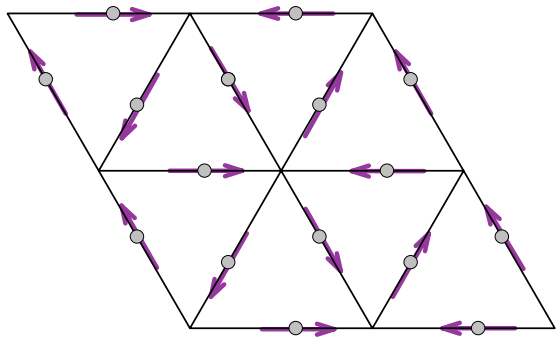

Fig. 3.3: *Ordering of the Er moments within the basal plane in ErNiAl compound.*

ErCuAl orders ferromagnetically below 6.8 K with the Er moments along the *c*-axis. The magnitude of the Er-moments reaches 6.7 μ_B at 1.8 K.

The erbium moments derived from neutron diffraction in both ErNiAl and ErCuAl are lower than the Er^{3+} free-ion value of 9 μ_B. The difference has been ascribed to the influence of crystal field (CF). Results of the study of CF excitations in ErNiAl are reported in [32].

$TbNi_{1-x}Cu_xAl$

The pseudo-ternary compounds $TbNi_{1-x}Cu_xAl$ has been studied by Ehlers et al. [3]. They crystallize in the ZrNiAl-type hexagonal structure within the whole concentration range of x [23,3]. The boundary concentrations (TbNiAl; TbCuAl) behave in the similar way as ErNiAl or ErCuAl, respectively.

The TbNiAl orders antiferromafnetically below the Néel temperature $T_N = 47$ K, with all Tb moments ordered. One third of Tb moments have considerably reduced magnitude compared to the remaining 2/3 of Tb moments [33]. There is another magnetic transition at $T_1 = 23$ K, which is connected with the change of propagation of the frustrated spins. All the Tb moments are of equal size of 8.1 μ_B at 2 K. On the other hand, TbCuAl is a simple ferromagnet with Tb moments along the c-axis with the magnitude of 7.7 μ_B [33]. All the Tb moments are of equal value at 2 K.

While increasing the concentration parameter x the lattice constants a and c raise systematically without any unexceptable change at 60 K [3]. Over the whole series $TbNi_{1-x}Cu_xAl$ the ordering temperature changes strongly with the Cu-concentration in the range from 25 K to 59 K (see *Fig. 3.4*). The Curie-Weiss temperature θ_p is positive for both the ferro- and antiferromagnetic compounds. In the range of $0.01 \leq x \leq 0.10$ the coexistence of ferro- and antiferromagnetic ordering

has been observed. This coexistence is not based on the idea of different parts of the sample with different type of alignment, but there should be "domains" in the whole compound which differ in the type of magnetic order (in the sense of volume with uniform type of order; not Weiss domains). Ferromagnetism has been found above the concentration of $x \geq 0.15$. The exception range of $0.60 \leq x \leq 0.80$ was marked as regime with a dominant short-range magnetic order. A change of the magnetic coupling mediated by *d* electrons (Ni rich part) to that mediated mainly by *s* electrons (Cu rich part) is proposed to explain observed data.

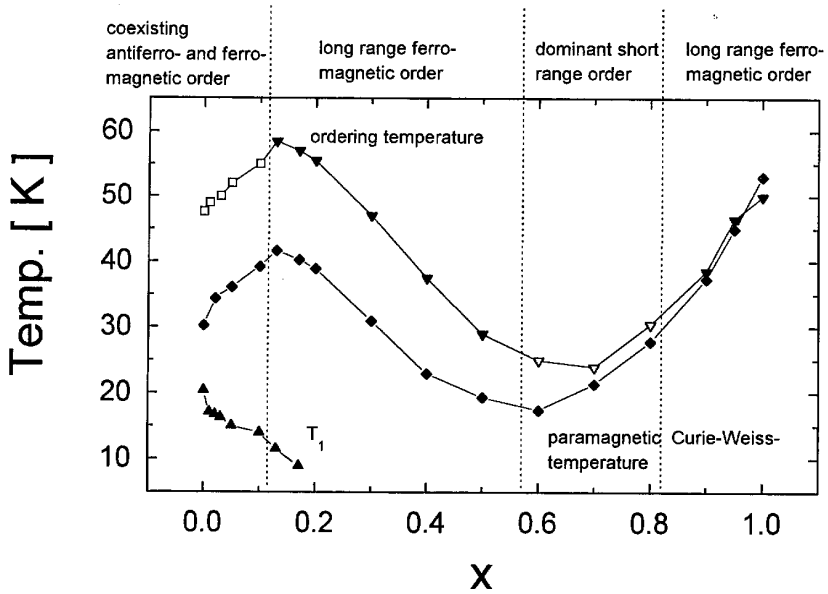

Fig. 3.4: *Ordering temperature, Curie-Weiss temperature and T_1 as they depend on the x-parameter in $TbNi_{1-x}Cu_xAl$ system [3].*

4. Experimental methods

4.1 Sample preparation

The polycrystalline samples have been prepared by arc-melting in mono-arc furnace under protection of argon atmosphere at pressure of 50 kPa after previous vacuum of 0.5-2 Pa.

The initial materials, which correspond to stoichiometric composition, consisted of pure elements with the purity of 99.9% for Er and Co, 99.995% for Ni and 99.999% for Cu and Al. In most cases there was used a little bit higher amount (0.5 to 1% added to the expected weight) of Al just because of higher evaporation during the melting. The samples have been turned and remelted three to four times to achieve better homogenity.

The samples with $x = 0.2$, 0.4 and 0.8 have been prepared in the same way as described above, already before this work. To achieve better quality, these samples were wrapped in a Ta foil and annealed for 10 days at 900 K.

Nevertheless, as x-ray and microprobe analysis showed, annealing had no effect on the improvement of the sample quality (see *5.1.2.* and *5.1.3.* sections).

4.2 Phase analysis

X-ray

All of the samples have been analysed by x-ray powder diffraction at room temperature with a conventional diffractometer (Siemens, installed at the Department of Electronic Structures at the Charles University) working with the Bragg-Bretano geometry.

The radiation of Cu (Co) with the wavelengths $\lambda(K\alpha_1) = 1.5405 \times 10^{-10}$ m and $\lambda(K\alpha_2) = 1.5445 \times 10^{-10}$ m ($\lambda(K\alpha_1) = 1.7889 \times 10^{-10}$ m, $\lambda(K\alpha_2) = 1.7928 \times 10^{-10}$ m, respectively) was used for the experiment. Additionally several samples ($x = 0.00$, 0.40, 0.50, 1.00) have been studied by x-ray powder diffraction in the temperature range from 3.7 K up to 296 K. Helium gas has been used as the cooling medium.

All the x-ray diffraction data have been analysed by the FullProf program [34], which enables to refine data from x-ray and neutron scattering. In an x-ray experiment, the structural parameters are refined from the positions and

intensities of the observed peaks. For a given crystal structure, positions of the nuclear reflections are given by the Bragg's law:

$$\lambda = 2d_{hkl} \sin\theta, \tag{4.1}$$

where λ is wavelength of the radiation, d_{hkl} is the distance of reflecting planes and θ is the angle between normal to the *hkl*–plane and the interacting x–ray.

Intensities of the reflected x–rays are proportional to the square of the structure factor

$$I \approx |F_{hkl}^2| , \tag{4.2}$$

where F_{hkl} is given by

$$F_{hkl} = f_{at} \exp(\mathrm{i}\boldsymbol{qr}) . \tag{4.3}$$

Here f_{at} is the atomic dispersion factor and it is equal to

$$f_{at}(\boldsymbol{q}) = \int_V \rho(\boldsymbol{r}) \exp(\mathrm{i}\boldsymbol{qr}) dr . \tag{4.4}$$

The parameter $\boldsymbol{q}$ is the position vector in the reciprocal space, the $\rho(\boldsymbol{r})$ stands for the charge density in the straight space at the position $\boldsymbol{r}$.

Microprobe

The microprobe analysis of selected samples has been performed at the Institute of Physics, Czech Academy of Sciences, using microanalyser JXA-733(JEOL). The following lines have been selected for the analysis of individual elements: Al-K_α, Cu-K_α, Er-K_α, Ni-L_α. The energy of the electron beam was 20keV. Pure Er, Cu, Al and Ni were used as standards. The weight concentrations have been obtained from the measured relative intensities (i.e. ratios to the standards) using a ZAF method [35] and a KEVEX program support [36].

The overall view of the surface of the samples has been obtained using COMPO-method. It uses the reverse-scattered electrons whose count is proportional

to the mean atomic number of the emitting area. This method is usually being used for resolution of the phases (hence COMPOsition).

4.3 Magnetization measurements

The samples for DC-magnetization measurements were made of powder consisting of randomly oriented grains fixed by nonmagnetic glue in a small ampule. The mass of powder sample was approximately 30-50mg.

All the low-temperature and some high-temperature (see *5.3.1*) dependencies of DC-magnetization, and all the magnetization curves have been measured at the Joint Laboratory of the Charles University and the Institute of Physics using the PPMS instrument, Quantum Design. Here, the magnetized sample is moved through the detection coils and induces a voltage in the detection coil set. The amplitude of this signal is proportional to the magnetic moment and the speed of the sample during extraction [37]. We have performed our measurements in the temperature region from 2 to 300 K, in external magnetic fields up to 5 T.

Additional measurements of high-temperature DC-magnetization data and some magnetization curves, to have a comparison with PPMS data for absolute measured values, have been measured on a SQUID magnetometer, Quantum Design, installed at the Institute of Physics of the Academy of Sciences of the Czech Republic. In this instrument the sample is situated in the centre of detection coils and after the lift along the coil axis within several steps the signals are read by the squid sensor. The magnetic moment of the sample is then determined from the flux changes in the superconducting loop (the flux variation is proportional to the magnetization of the sample). The system can detect a magnetic moment with the sensitivity of 10^{-11} A.m^2 in magnetic fields up to 5 T. For our measurements we have used the temperature range between 4.8 and 300 K.

4.4 Specific heat

The specific heat experiments were performed using the PPMS instrument. Measurements were done on polycrystalline samples with the weight of 20-30 mg. One surface of the sample was adjusted to a straight plane by which was the sample then connected to heat capacity measuring system. After reaching high vacuum in the sample space it is thermally isolated and cooled to the required temperature *T*. Then it is stepwise heated in several measurement cycles. In each cycle a known

amount of heat is added to the sample and the reach of the temperature ΔT is indicated. The average heat capacity $\overline{C_P}$ is then determined as

$$\overline{C_P} = \Delta Q/\Delta T \tag{4.5}$$

When the ratio $\Delta T/T$ is small, $\overline{C_P}$ is almost equal to the theoretical value which is defined as $C = \mathrm{d}Q/\mathrm{d}T$. The PPMS software uses the two-tau relaxation method to determine the heat capacity values (for more details see [37]).

5. Results

5.1 Structure analysis

5.1.1. ZrNiAl-type structure

The studied materials belong to the group of ternary intermetallic *RTX* compounds crystallizing in ZrNiAl-type hexagonal structure (space group $P\bar{6}2m$; group No. 189; *Fig. 5.1a*). *R* stays here for a rare-earth metal, *T* is a transition metal and *X* stands for IIIB, IVB or VB group of the Periodic Table of Elements.

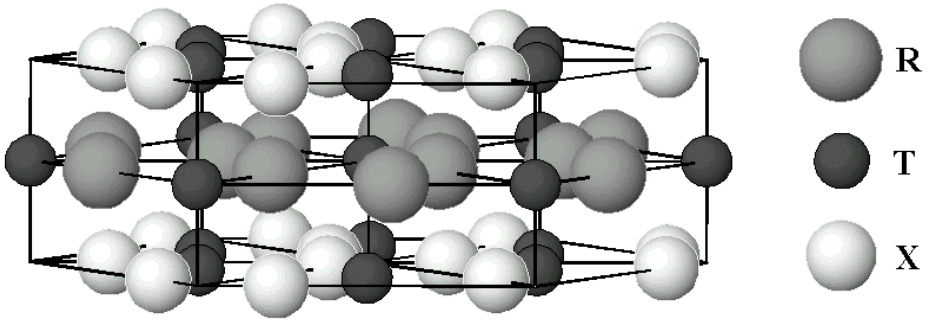

Fig. 5.1a: *ZrNiAl-type hexagonal structure.*

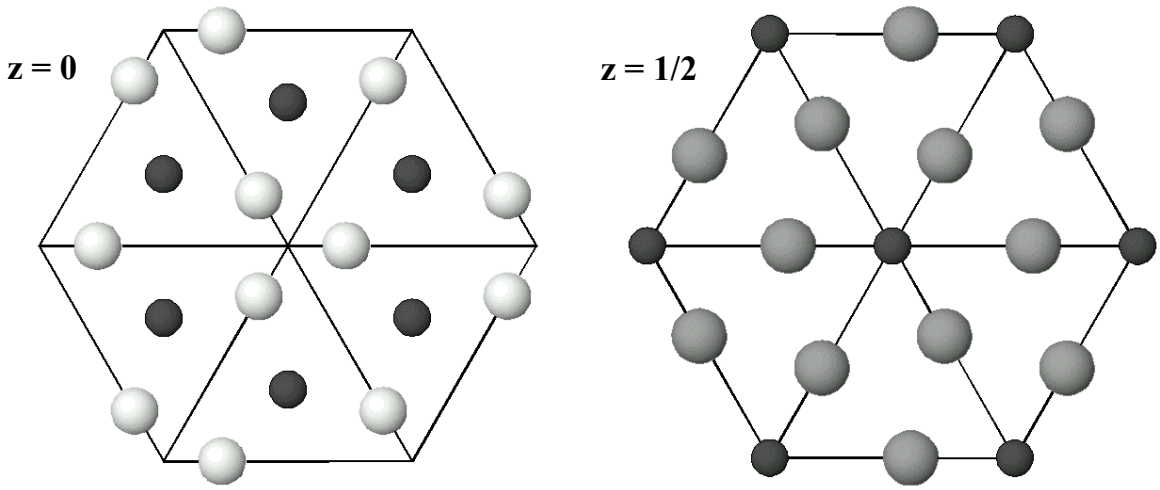

Fig. 5.1b: *Two types of basal planes in ZrNiAl-type structure.*

There are two types of planes in the ZrNiAl-type hexagonal structure (*Fig. 5.1b*). One type of the basal planes contains the rare earth (*R*) and one out of three atoms of the transition metal (*T*) per unit cell. Two such layers are separated by a non-magnetic layer containing *p*-metal (*X*) and two out of the three transition

metal atoms (*T*). These two planes change periodically in the ABAB… sequence. The coordinates of the elements are following:

3*R* : (X, 0, 1/2), (0, X, 1/2), (-X, -X, 1/2) 2*T* : (1/3, 2/3, 0), (2/3, 1/3, 0)
3*X* : (Y, 0, 0), (0, Y, 0), (-Y, -Y, 0) 1*T* : (0, 0, 1/2)

While the positions of transition-metal atoms are fixed, the positions of rare-earth and *p*-metal atoms depend on structure parameters *X* and *Y*. Values of these parameters are obtained from x-ray analysis (see *Table 5.1*).

As it is seen from the *Fig. 5.1* each of the *R* atoms has four nearest neighbours of the similar element in the same basal plane at a distance

$$d = a\sqrt{1 - 3X + 3X^2} \tag{5.1}$$

Another two neighbours lie in the nearest plane of the same type at a distance of the lattice constant *c*. The ratio *c*/*a* determines which of these two types of neighbours is the nearest neighbour, eventually.

5.1.2. X-ray

$ErNi_{1-x}Cu_xAl$

The x-ray powder diffraction analysis at room temperature attested the structure and phase composition. All the samples crystallize in the ZrNiAl-type hexagonal structure (sec. *5.1.1.*).

To compare the annealed samples with the samples, which have not been annealed, we show *Fig. 5.2a* (annealed) and *Fig. 5.2b* (without annealing). Both of them embody comparable quality of the studied pollycrystals. Consequently we can say that the annealing has no substantial influence on the crystal structure quality.

We have found out that in each sample diffraction pattern appears one extra peak at the position $2\theta \approx 50.1°$ (using Co-radiation). It corresponds to the second strongest peak in $ErCu_2$ compound. The strongest peak of $ErCu_2$ is at the position that corresponds to one of strongest peaks of our compounds, so it may overlap with this reflection peak.

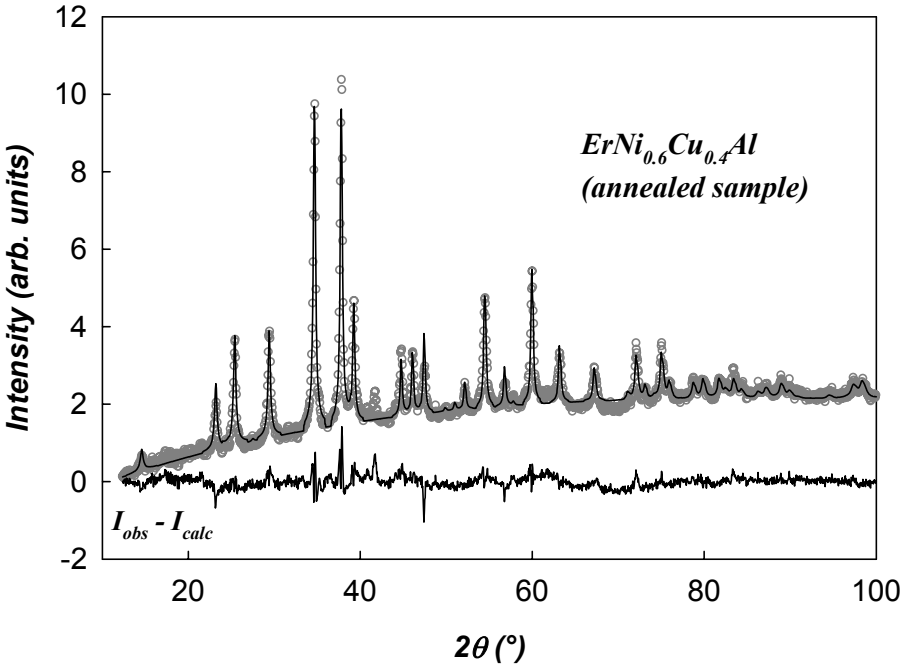

Fig. 5.2a: *The powder diffraction pattern of one of the annealed samples, x = 0.40. This pattern has been obtained using Cu radiation.*

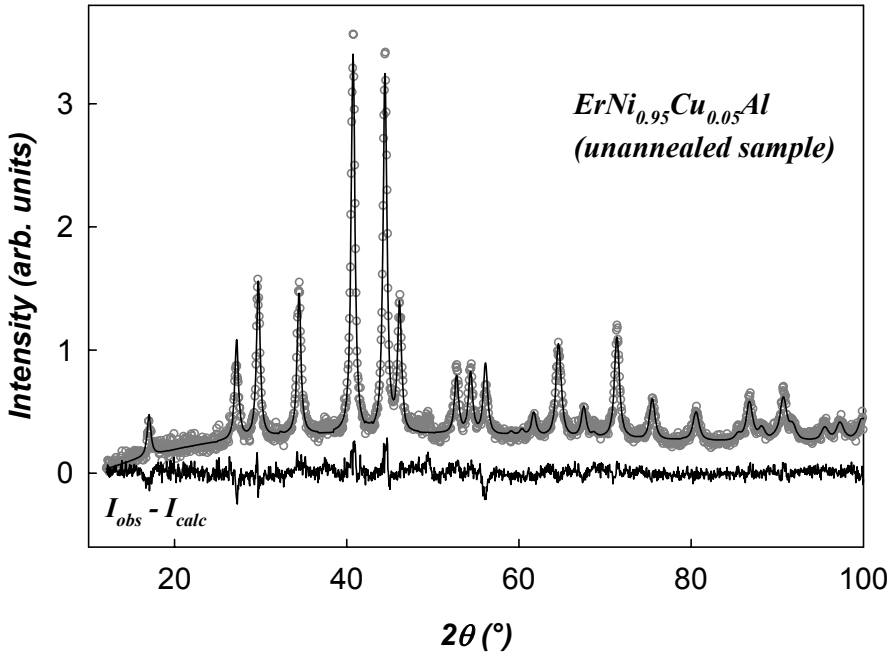

Fig. 5.2b: *The powder diffraction pattern of one of the unannealed samples, x = 0.05. Open circles represent the observed values, solid line is the calculated profile (refined by the program FullProf as described in sec. 4.2). The plot of the difference between observed (I_{obs}) and calculated (I_{calc}) values is added. This record has been obtained using Co lamp. The pattern has been obtained in the range up to $2\theta = 150°$. In Figs. 5.2a,b we display lower angle range for better resolution.*

Table 5.1 contains concentration dependence of the lattice parameters at the room temperature. These data are displayed in *Fig. 5.3*. It is seen that parameters *a* and *c* are liable to reasonable tendency until the concentration of copper is about 50% (i.e. $x = 0.50$). At this point the lattice parameters suddenly change and by continuing to higher *x* follow the tendencies as before this 'jump'. By viewing the *Fig. 5.3* it is also clear that there is no break away from the linear increase of the volume per formula unit. So the 'jump' of the lattice constants *a* and *c* is not connected with any change of the volume of the lattice cell.

Table 5.1: *Lattice parameters of $ErNi_{1-x}Cu_xAl$ and several of $ErNi_{1-y}Co_yAl$ samples at room temperature.*

x	a (pm)	c (pm)	X_{Er}	X_{Al}
0.00	696.9 ± 0.5	380.1 ± 0.3	0.584 ± 0.003	0.203 ± 0.018
0.05	698.0 ± 0.1	380.6 ± 0.1	0.584 ± 0.001	0.214 ± 0.005
0.10	698.8 ± 0.2	380.7 ± 0.1	0.585 ± 0.001	0.213 ± 0.007
0.20	699.9 ± 0.2	381.3 ± 0.1	0.585 ± 0.001	0.209 ± 0.009
0.40	701.3 ± 0.3	383.3 ± 0.2	0.584 ± 0.002	0.209 ± 0.011
0.50	701.8 ± 0.9	385.4 ± 0.5	0.583 ± 0.004	0.184 ± 0.020
0.60	692.8 ± 0.2	398.6 ± 0.1	0.584 ± 0.001	0.232 ± 0.009
0.80	694.4 ± 0.2	399.9 ± 0.1	0.582 ± 0.001	0.185 ± 0.009
1.00	697.6 ± 0.5	401.6 ± 0.4	0.588 ± 0.003	0.190 ± 0.023
0.10 (Co)	697.3 ± 0.5	380.9 ± 0.4	0.581 ± 0.003	0.199 ± 0.025
0.20 (Co)	696.5 ± 0.7	381.5 ± 0.5	0.581 ± 0.006	0.195 ± 0.041

The structural parameters X_{Er} and X_{Al} determining the positions of rare-earth and *p*-metal are on the other hand independent on the concentration *x* within the error range, so it can be said that these positions are stable.

$ErNi_{1-y}Co_yAl$

The structural study by the means of x-rays showed that the series $ErNi_{1-y}Co_yAl$ changes its crystal structure from the ZrNiAl-type just by substituting 20% of cobalt instead of nickel. In this sample several foreign peaks appear. Therefore values for this sample are of lower certainty, in *Figure 5.3* we mark them with *.

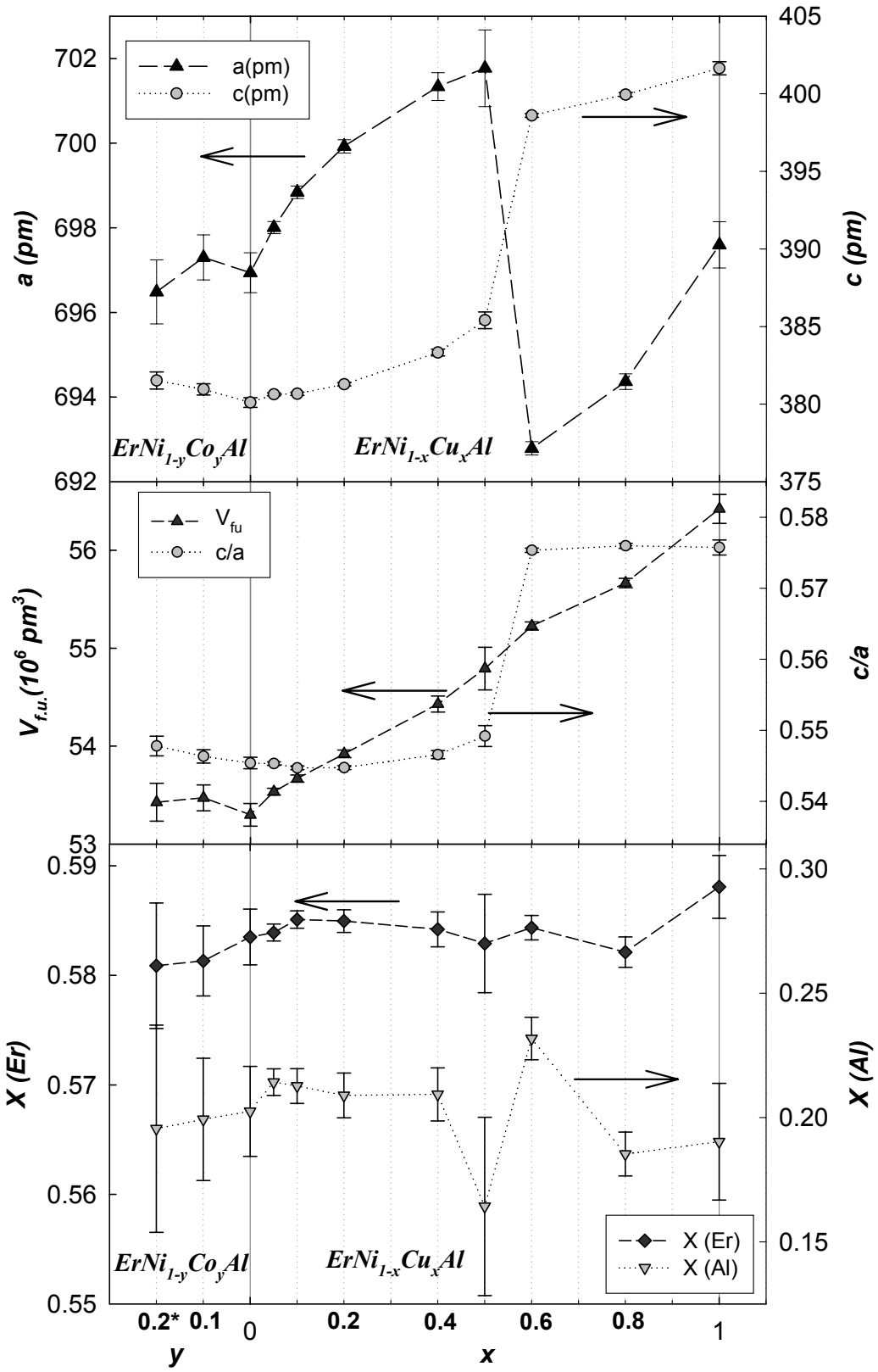

Fig. 5.3: Concentration dependence of the lattice constants in $ErNi_{1-x}Cu_xAl$ and $ErNi_{1-y}Co_yAl$ (for y = 0.1 and 0.2) at room temperature.*

5.1.3. Microprobe experiment

Three samples ($x = 0.05$; 0.40; 0.80) have been studied by the microprobe analysis. We verified that distribution of individual elements is homogenous.

The microprobe analysis showed that the samples consist of four different phases (see *Fig. 5.4* and *Table 5.2*). In addition to the main phase there are two impurity phases and also some pieces of Ta on the studied surface. First one (impurity phase 1) is in all cases composed of pure erbium, another one (impurity phase 2) consists of all original elements. The amount of all impurities is much smaller than that of the main phase (*Fig. 5.4*).

The main phase is composed of the amount of the individual elements as that given by stoichiometric formula (within the rightness range of this method) for $x = 0.05$ and 0.80. Small excess of Er and lack of Al is found in the $x = 0.40$ sample. There are two types of error, which should be considered in this method. First one is the accuracy depending on the statistical dispersion of values obtained from individual photons. Also error due to inaccuracy in counting patterns of standards is included in this error type. It is not higher than 1% of element composition in the material. Another type of error is the accuracy, which depends on the used model. It is about 3% of the element composition.

Table 5.2: *The composition of individual phases in the $ErNi_{1-x}Cu_xAl$ for $x = 0.05$; 0.40 and 0.80 obtained by the microprobe experiment.*

		Weight fraction (in %)				Atomic fraction (in %)			
Sample	Phase type	Er	Ni	Cu	Al	Er	Ni	Cu	Al
$x = 0.05$	Main phase	68.9	21.2	0.7	10.8	34.8	30.6	1.0	33.7
	Impurity phase 1	86.4	1.5	0.0	0.2	94.1	4.6	0.0	1.2
	Impurity phase 2	46.1	38.2	2.1	13.6	18.8	44.5	2.3	34.4
$x = 0.40$	Main phase	67.8	14.4	5.7	7.5	39.7	24.1	8.9	27.3
	Impurity phase 1	86.5	0.5	0.0	0.0	98.3	1.5	0.0	0.2
	Impurity phase 2	43.0	14.4	26.7	11.1	19.2	18.4	31.5	30.9
$x = 0.80$	Main phase	67.0	4.8	15.8	10.7	35.5	7.2	22.0	35.3
	Impurity phase 1	80.5	0.3	0.0	0.1	98.1	1.0	0.0	0.9
	Impurity phase 2	41.9	2.4	39.7	11.1	18.9	3.1	47.1	31.0

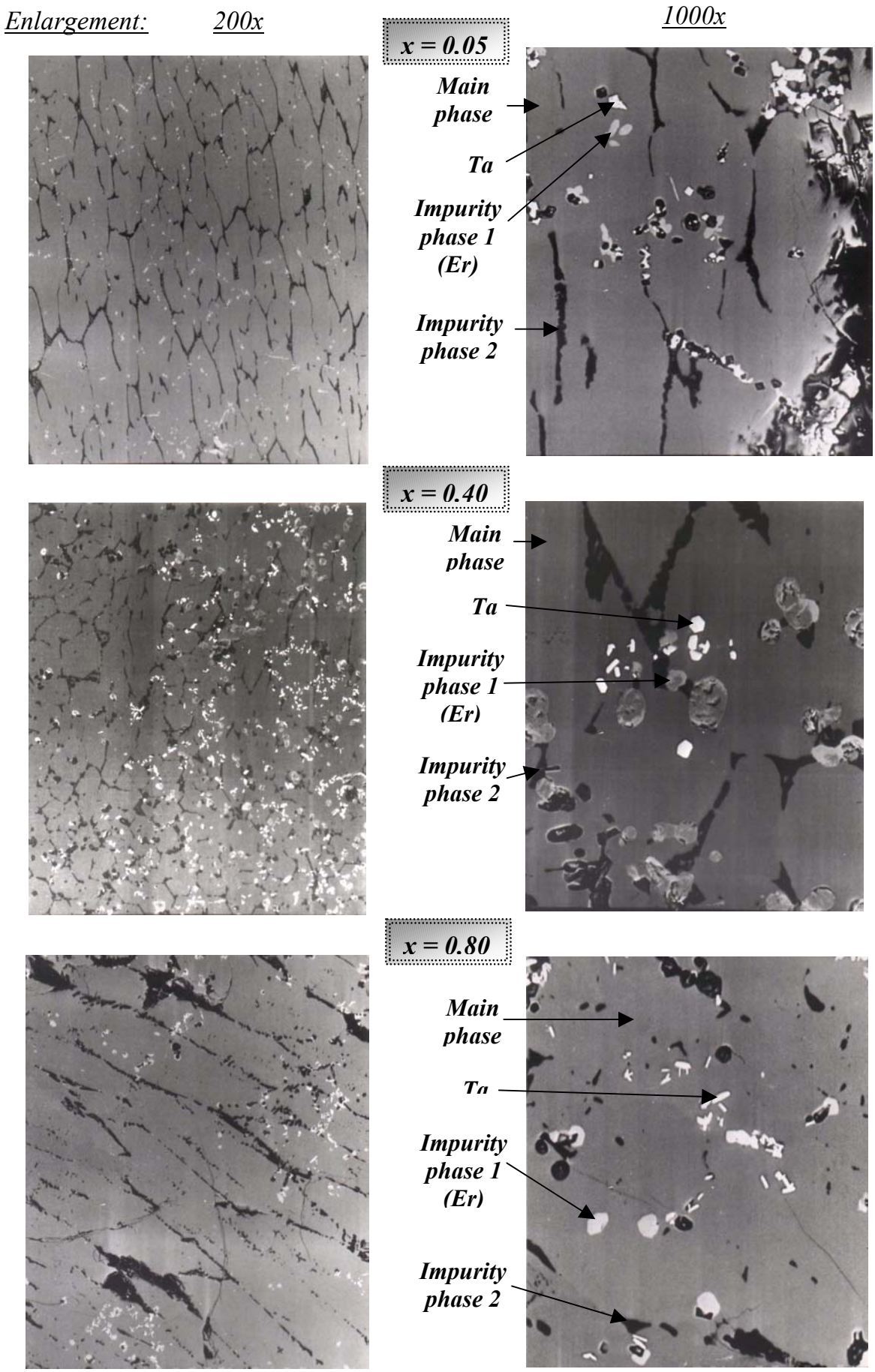

Fig. 5.4: *Photographic zooms of surfaces of samples studied by the microprobe. The pictures have been obtained in COMPO regime, i.e. by back-up scattered electrons.*

The impurity phase 2 represents compound with the composition like $Er_{0.2}([Ni,Cu])_{0.5}Al_{0.3}$. This type of impurity has been observed also in the boundary compound ErCuAl [1] marked as 'impurity phase 2'. Presence of this impurity might be possible origin of the extra peak observed in our x-ray diffraction data. It is more likely explanation than the $ErCu_2$ reflection because no traces of $ErCu_2$ are observed in the microprobe analysis.

The Ta impurity comes from the annealing procedure, when the samples have been annealed in a tantalum foil. Then the Ta atoms could evaporate from the foil and cover the surface of the annealed sample. It is also possible that they have diffused into the small depth under the surface of the sample. Nevertheless, Ta is nonmagnetic material, so it cannot influence our results.

We shall mention that also the boundary compound ErCuAl contained similar amount of impurities, which have no influence on the observed magnetic properties [1].

5.2 Thermal expansion

The lattice parameters of several samples ($x = 0.0$; 0.4; 0.5 and 1) from the series $ErNi_{1-x}Cu_xAl$ have been studied in the temperature region of 5-300 K. The concentration dependence at 50 K and 5 K, compared with the concentration dependence at the room temperature is shown in the *Table 5.3* and *Figure 5.5*. Although the whole concentration range had not been studied at this temperature, it is almost clear, that the lattice parameters follow the same type of concentration dependence as that at the room temperature. The only differences can be a slightly reduced values of the *a*- and *c*-parameters. It is visible that the *a*- and *c*-constants at 5 K correspond (within the error) to that obtained at the temperature of 50 K.

Tab. 5.3: *The lattice parameters of the $ErNi_{1-x}Cu_xAl$ series for x = 0.0; 0.4; 0.5 and 1.0 at T = 50 K.*

x	a (pm)	c (pm)	X_{Er}	X_{Al}
0.0	694.9 ± 0.6	379.8 ± 0.4	0.583 ± 0.003	0.22 ± 0.02
0.4	700.1 ± 0.6	382.9 ± 0.2	0.584 ± 0.002	0.21 ± 0.01
0.5	700.2 ± 0.4	385.5 ± 0.3	0.587 ± 0.002	0.21 ± 0.03
1.0	696.3 ± 0.5	400.6 ± 0.4	0.588 ± 0.002	0.19 ± 0.02

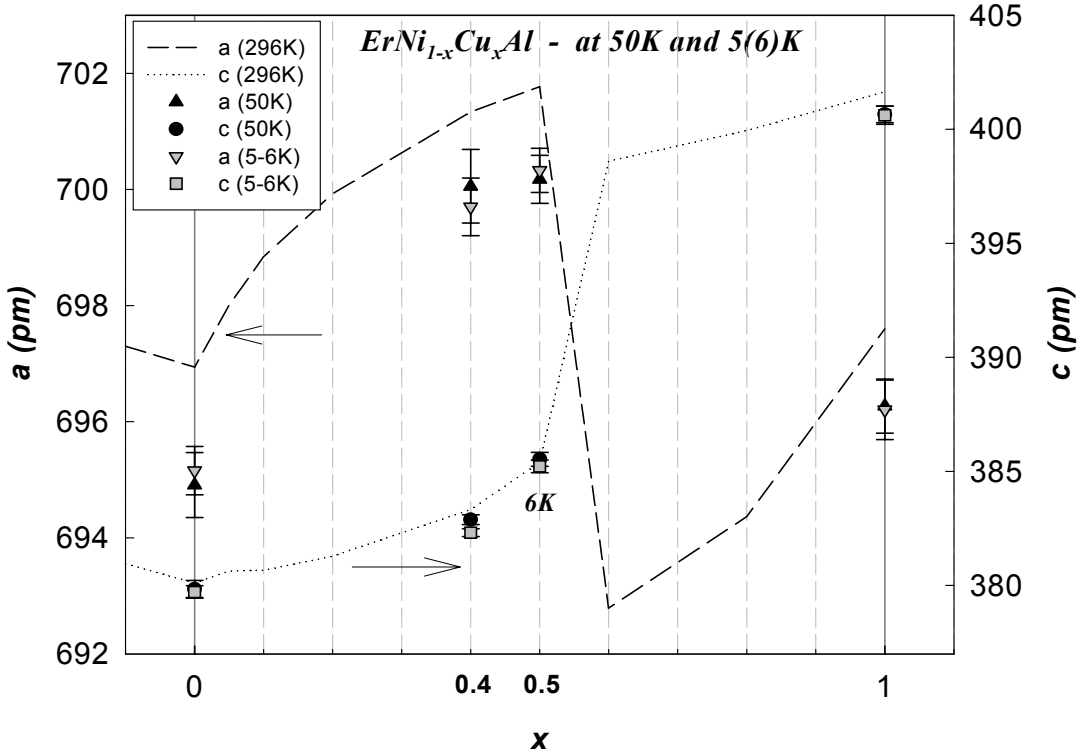

Fig. 5.5: *The concentration dependence of lattice parameters in $ErNi_{1-x}Cu_xAl$ series for x = 0; 0.4; 0.5 and 1 at T = 50 K and 5 K (6 K for the x = 0.5 compound). The dashed and dotted line represents the concentration dependence of a- and c-constant at the room temperature, respectively.*

In contrast to the series $TbNi_{1-x}Cu_xAl$, where the lattice parameters increase monotonically with the parameter x within the whole series [3] at the temperature of 60 K, our results (obtained at 50 K) show lattice jump between $x = 0.5$ and 0.6, similar to room temperature dependence.

While viewing the temperature dependencies of lattice parameters (*Figs. 5.6* to *5.9*) it could be said that these do not change within the temperature range and the values are mostly the same in relation to the error bars. But it is also visible that some correlation between temperature and the lattice constants occurs. With the increasing temperature the mean value of parameter c increases until the temperature reaches the value of 60-80 K and after that this lattice constant is relatively stable. On the other hand, a decreases in a small temperature range within the low-temperature region, at about 30-50 K gets minimum and after that appreciably grows up. It is evident that the increase of the a-parameter begins at approximately the same temperature as the 'saturation' of the c-parameter is reached.

Tendencies of these changes are most prominent for the samples of $x = 0.40$ (*Fig. 5.8*), while in ErCuAl we can observe just monotonous increasing of both lattice constants from low- up to room-temperature (*Fig. 5.9*).

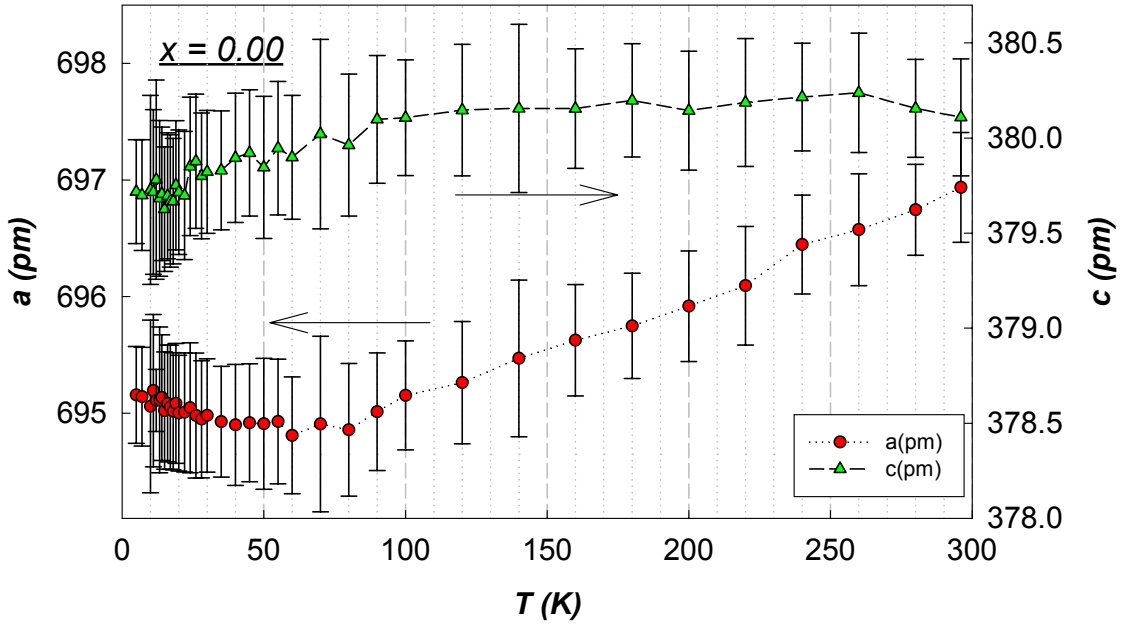

***Fig. 5.6**: The evolution of lattice parameters a and c in ErNiAl compound within the temperature range of 5-296 K.*

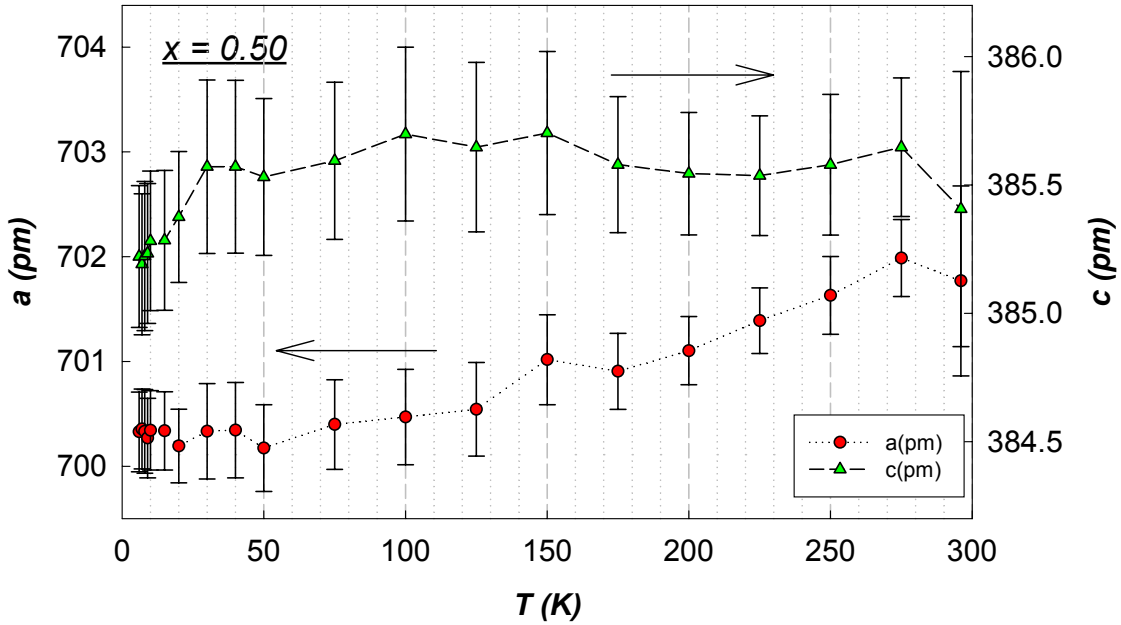

***Fig. 5.7**: The evolution of lattice parameters a and c in $ErNi_{0.5}Cu_{0.5}Al$ compound within the temperature range of 6-296 K.*

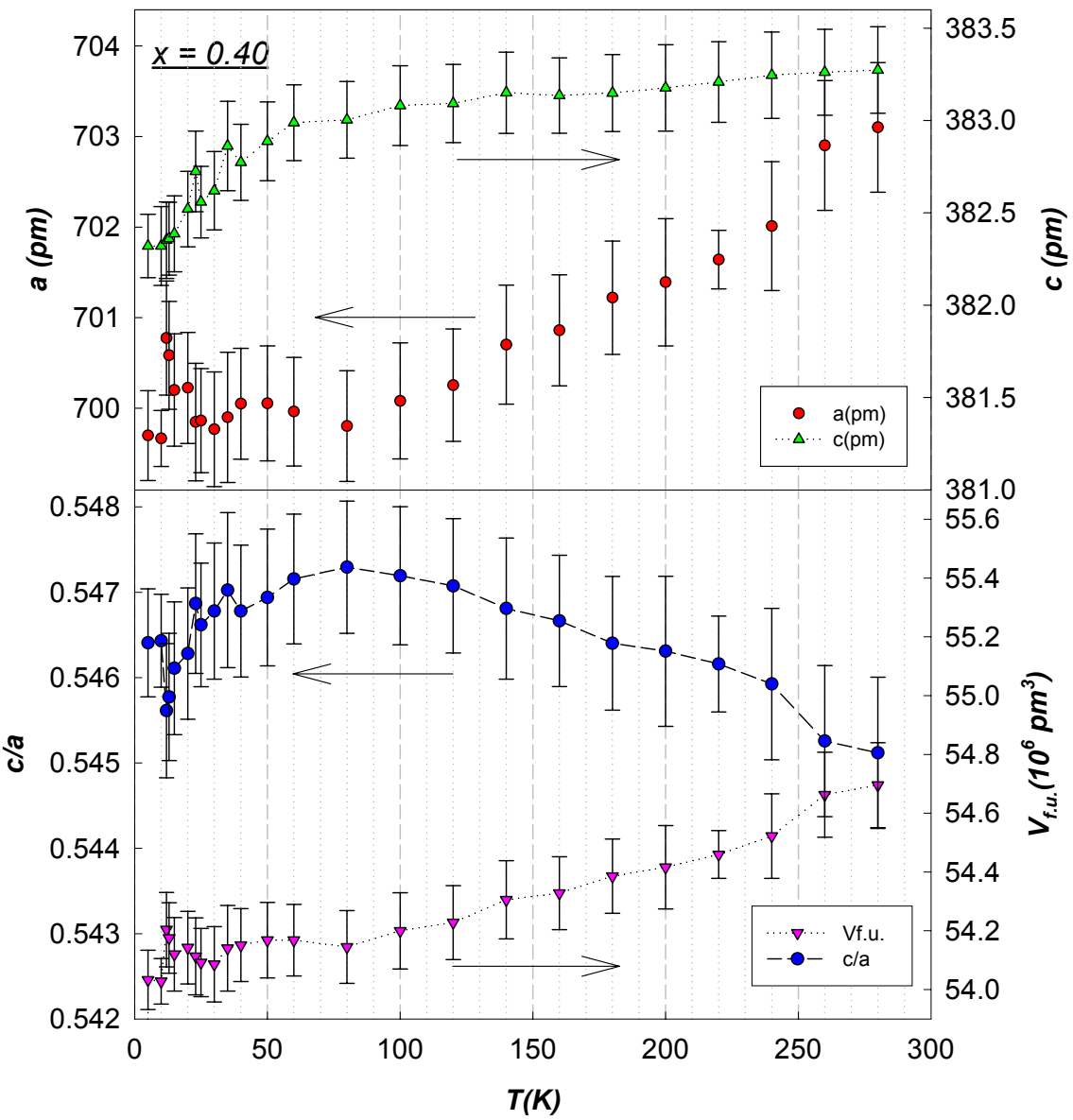

Fig. 5.8: *The evolution of lattice parameters a and c, the ratio of the lattice parameters c/a and of the volume per formula unit in the* $ErNi_{0.6}Cu_{0.4}Al$ *compound within the temperature range of 5-296 K.*

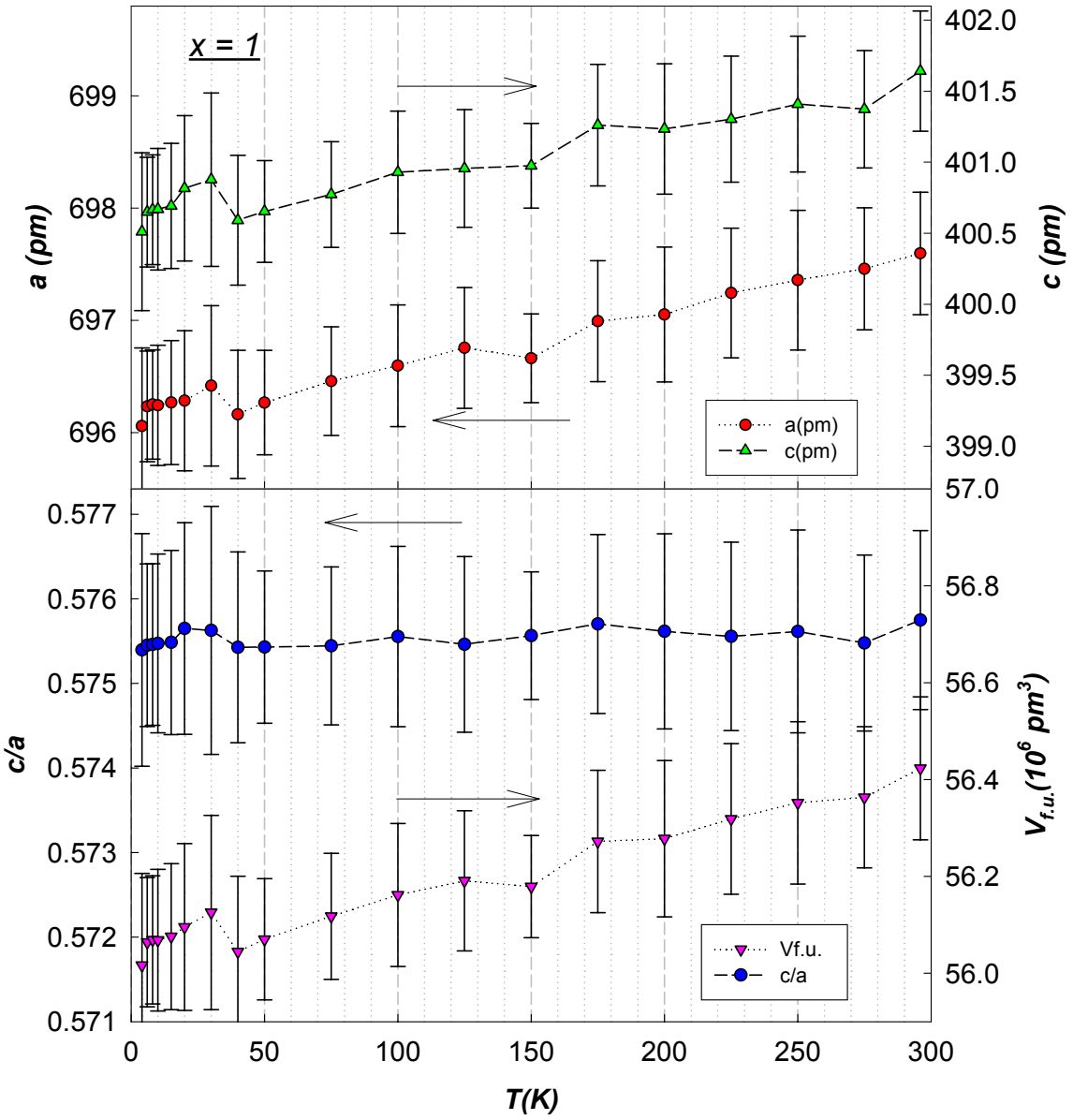

Fig. 5.9*: The evolution of lattice parameters a and c, the ratio of the lattice parameters c/a and of the volume per formula unit in the ErCuAl compound within the temperature range of 5-296 K.*

5.3 Magnetic study

5.3.1 High-temperature susceptibility

The magnetic susceptibility follows the Curie-Weiss dependence in the paramagnetic region, and can be fitted to the expression:

$$\chi = \frac{M}{H} = \frac{N_A \mu_0 \mu_B^2 \mu_{eff}^2}{3k_B(T-\theta_p)} + \chi_0 = \frac{C}{(T-\theta_p)} + \chi_0 . \qquad (5.2)$$

Here, μ_{eff} is the effective magnetic moment, θ_p is the paramagnetic Curie temperature, C stands for the Curie constant. The other symbols are constants usually used: N_A and k_B are the Avogader's and the Boltzmann's number, respectivelly, μ_B stands for the magnitude of the Bohr's magneton and μ_0 is the permeability of the vacuum. The parameter χ_0 is temperature independent. Because it includes the Pauli-paramagnetic contribution but is also influenced by the experimental setting, it has no deeper physical meaning. The values of χ_0 have been found close to zero in all our fits.

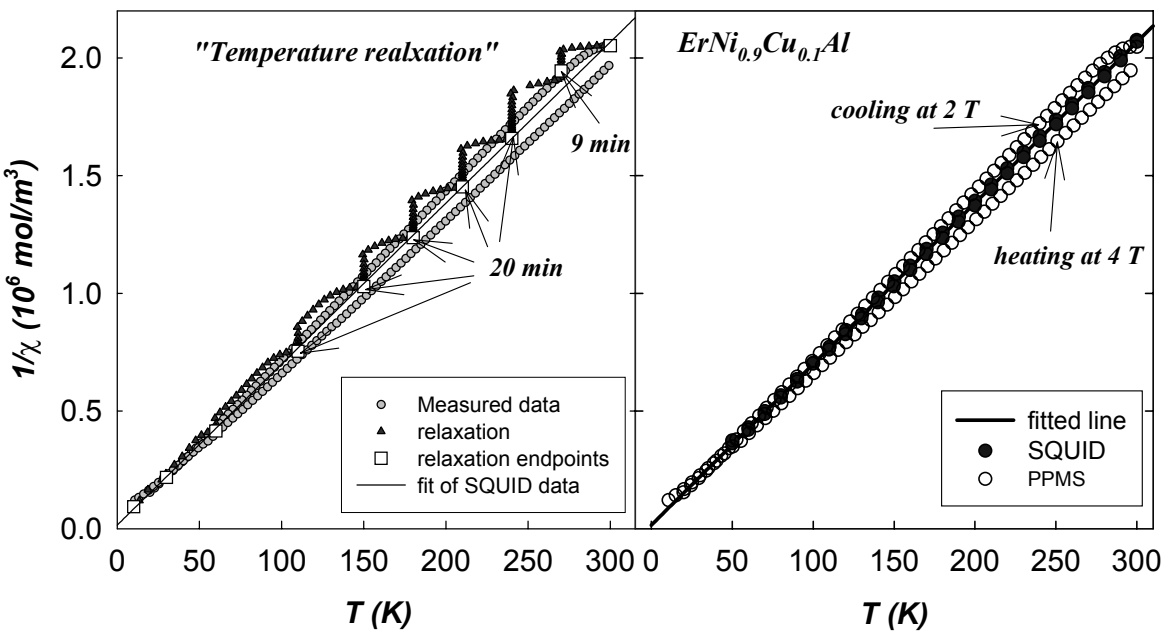

Fig. 5.10: *The high temperature susceptibility values (the right figure) fitted by the Curie-Weiss law (5.2). The solid line represents the fit, the empty symbols are the data measured usingPPMS added for comparison (see text). The left figure shows "relaxation" due to stabilization of the temperature between the sample and the thermometer in PPMS. The squares symbolize the last point measured before setting of the next temperature (i.e. at the end of the "relaxation").*

The necessary parameters μ_{eff} and θ_p have been obtained by fitting the experimental *H/M* vs. *T* data with the equation (5.2). The data measured by the SQUID instrument have been used for this. For an illustration, we show the data obtained for $ErNi_{0.9}Cu_{0.1}Al$ in *Fig. 5.10*. The fit to experimental data is represented by the solid line. The hollow circles represent the values obtained using the PPMS instrument. The difference between data obtained when cooling and heating has been caused by too high speed of the measuring regime, which was 2 K/min. The temperature given by the thermometer did not correspond to the actual sample temperature. It might be also caused by bad calibration of the thermometer. Additional measurements showed that waiting for several minutes gives more reasonable values corresponding to the state when the temperature was already being stabilized and corresponds to that on the sample (see the empty squares in the left side part of the *Fig. 5.10*).

The parameters μ_{eff} and θ_p derived from the least square fit of the equation (5.2) are given in *Tab. 5.4* and *Fig. 5.11*. In comparison to the theoretical value of the free ion (μ_{eff} (Er^{3+}) = 9.59) only the concentrations of $x = 0.00$; 0.10; 0.80; 1.00 and $y = 0.10$ correspond to the expected values. The other numbers are slightly higher.

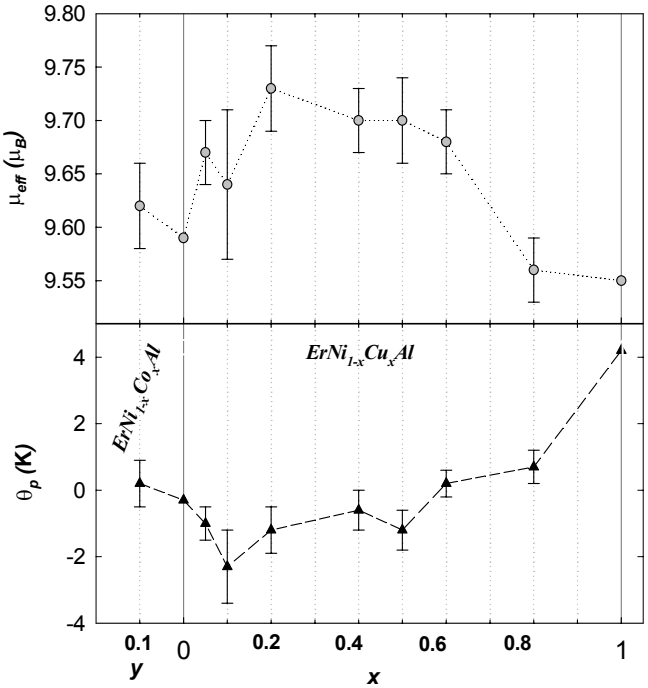

Fig. 5.11: *The concentration dependence of the effective momenta (μ_{eff}) and the Paramagnetic Curie temperature (θ_p) for the $ErNi_{1-x}Cu_xAl$ series and the $ErNi_{0.9}Co_{0.1}Al$ sample.*

Table 5.4: *The parameters μ_{eff}, and θ_p obtained by fitting the measured data to Eq. 5.2 for the $ErNi_{1-x}Cu_xAl$ series and for the $ErNi_{0.9}Co_{0.1}Al$ sample. The data for ErNiAl and ErCuAl have been taken from Refs. [1,2].*

x	μ_{eff} (μ_B)	θ_p (K)
0.00[2]	9.59	-0.3
0.05	9.67 ± 0.03	-1.0 ± 0.5
0.10	9.64 ± 0.07	-2.3 ± 1.1
0.20	9.73 ± 0.04	-1.2 ± 0.7
0.40	9.70 ± 0.03	-0.6 ± 0.6
0.50	9.70 ± 0.04	-1.2 ± 0.6
0.60	9.68 ± 0.03	0.2 ± 0.4
0.80	9.56 ± 0.03	0.7 ± 0.5
1.00[1]	9.55	4.2
0.10 (Co)	9.62 ± 0.04	0.2 ± 0.7

5.3.2 0.05 ≤ x ≤ 0.20: two phase transition region

The low-temperature DC-magnetization dependencies have been measured as described in sec. 4.3. All the samples have been studied in small external field of 0.01 T and additionally in some larger fields.

In the heat capacity data the phase transition can be found by idealization of the specific heat jump, while the magnetic entropy is necessary to be conserved.

The possible points of phase transition temperatures are summarized in the *Table 5.5a,b* at the end of this subsection.

The compounds with low Cu-concentration (x ≤ 0.2) exhibit two maxima in temperature dependencies of magnetization. The maximum in the curve measured in the field-cooled regime indicates an antiferromagnetic-type phase transition. The 5%-Cu sample has the maxima at 5.5 and 4.5 K. The heat capacity data confirm the phase transitions of the compound with 5% of substituted copper at temperatures of 5.7 and 4.4 K (see *Fig. 5.12* and *Table 5.5*). There is visible one weak anomaly more in the heat capacity data at T = 3.4 K. It is probably caused by the erbium impurities that can be present in the form of oxide.

The samples with $x = 0.10$ and 0.20 embody at least two phase transitions according to the maxima in the magnetization (*Fig. 5.13*), similar to $x = 0.05$. While increasing the parameter x, these anomaly points are shifted to lower temperatures. The field-cooled (fc) magnetization in the compound $ErNi_{0.90}Cu_{0.10}Al$ has no maximum, although the anomalies are visible. The maxima of zero-field cooled (zfc) curves (that are at corresponding temperatures) have been taken to derive the values of 4.9 and 4.4 K. Thus the ferromagnetic admixture cannot be foreclosed. The 20% Cu-substituted sample shows the maxima at 4.3 and 3.1 K.

The magnetization curves measured at different temperatures embody two-direction curvatures at the temperature of 2 K. This is typical for antiferromagnetically ordered materials. As it is seen, this effect is lowered for compounds with higher x (*Fig. 5.14*). It may be connected with an existence of ferromagnetic component, which is increasing with increasing x. We have measured several magnetization curves also using the SQUID magnetometer to ensure the absolute values are the same as that from PPMS. Good agreement has been observed.

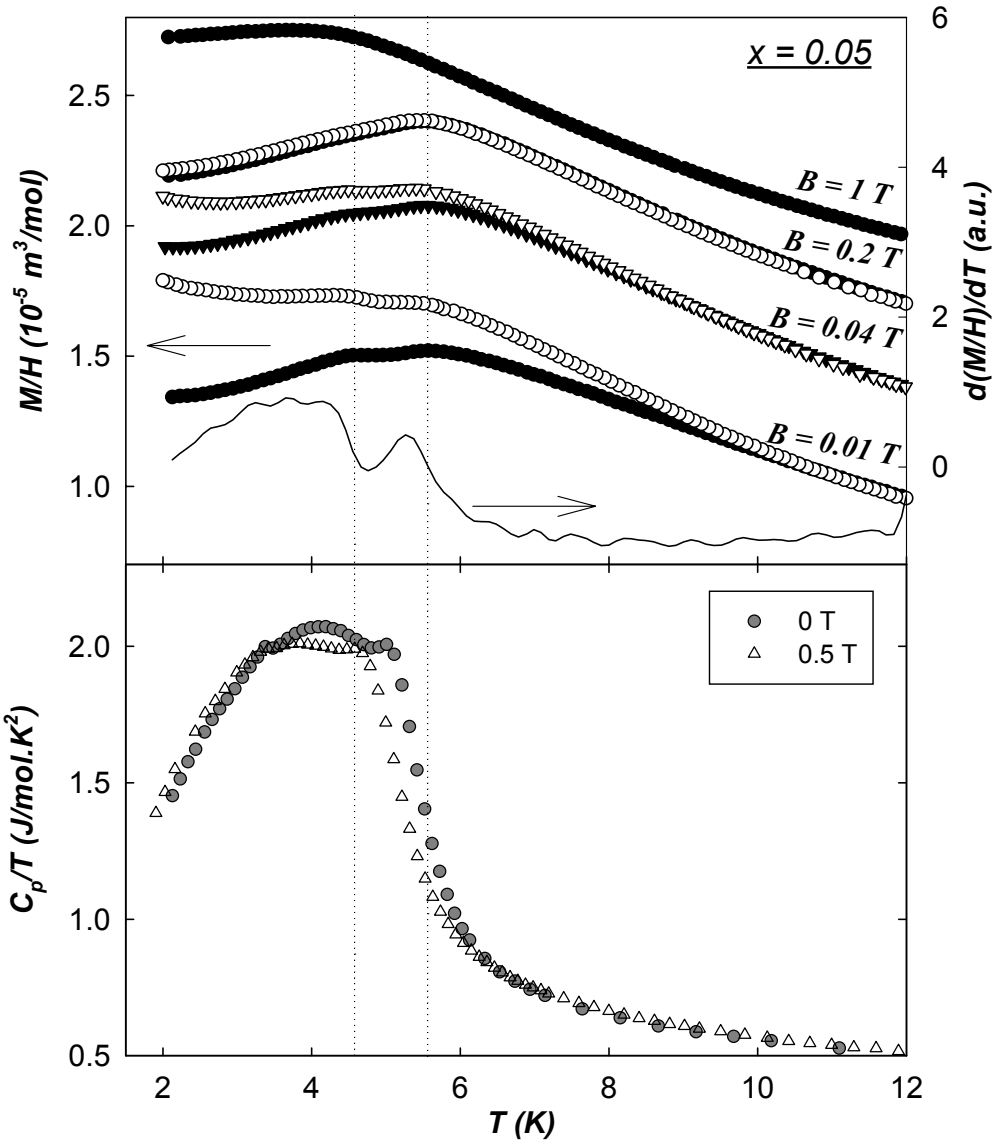

***Fig. 5.12**: The temperature dependence of M/H and C_p in the low temperature region for the $ErNi_{0.95}Cu_{0.05}Al$ sample measured in different magnetic fields with regime field-cooled (open symbols) and zero field-cooled (full symbols). The first derivative of zero field-cooled data in 0.01 T is represented by the solid line. The dependencies in larger fields are shifted because of better view. The heat capacity data measured in the external magnetic field of 0.5 T are represented by empty triangles. The vertical dotted lines represent the possible magnetic ordering temperatures.*

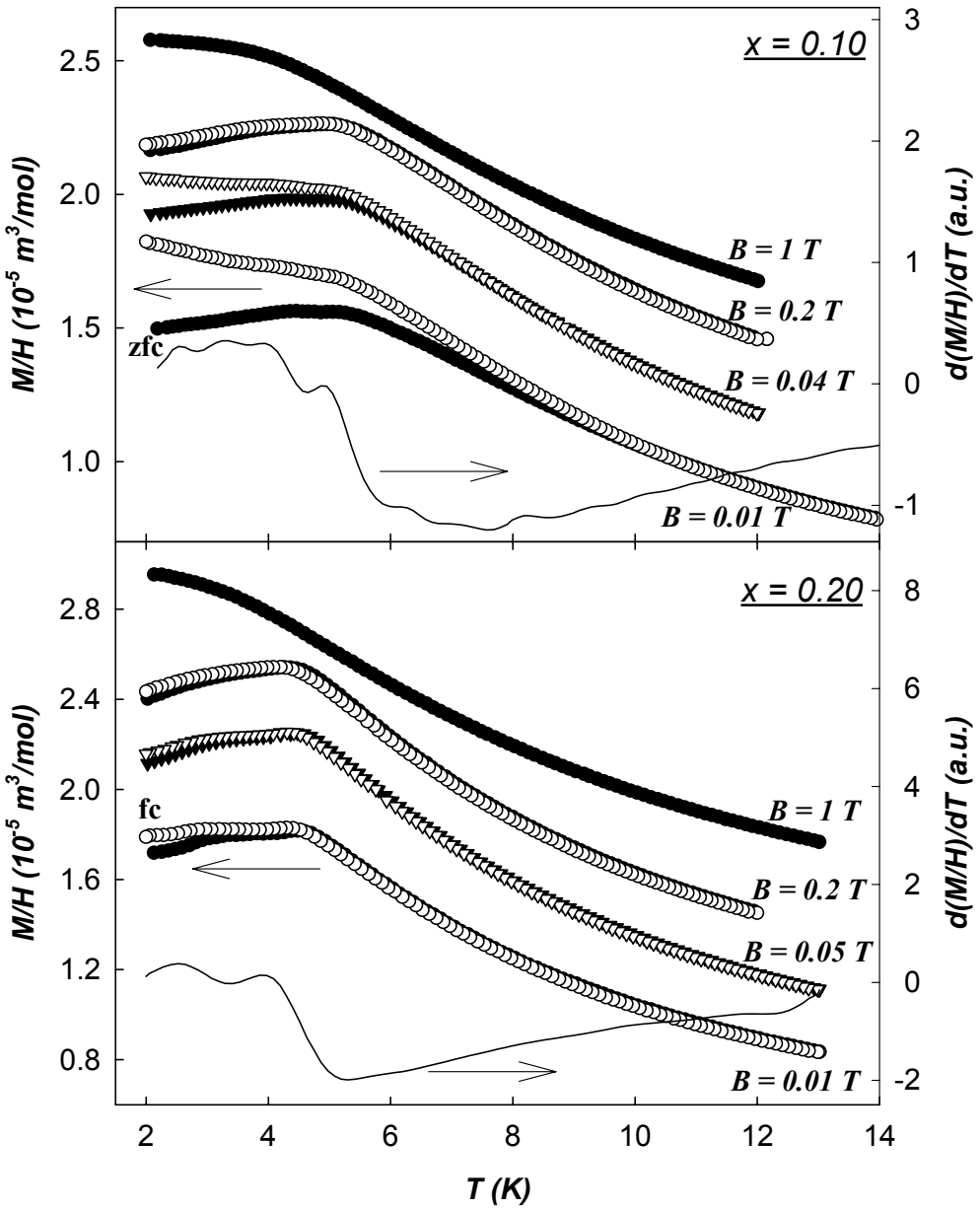

Fig. 5.13*: The temperature dependence of M/H in the low temperature region for the samples with x = 0.10 and 0.20 measured in different magnetic fields with regime field-cooled (open symbols) and zero field-cooled (full symbols). The first derivatives of zero field-cooled (zfc, for 0.10) and field-cooled (fc, for 0.20) data in 0.01 T are represented by the solid lines.*

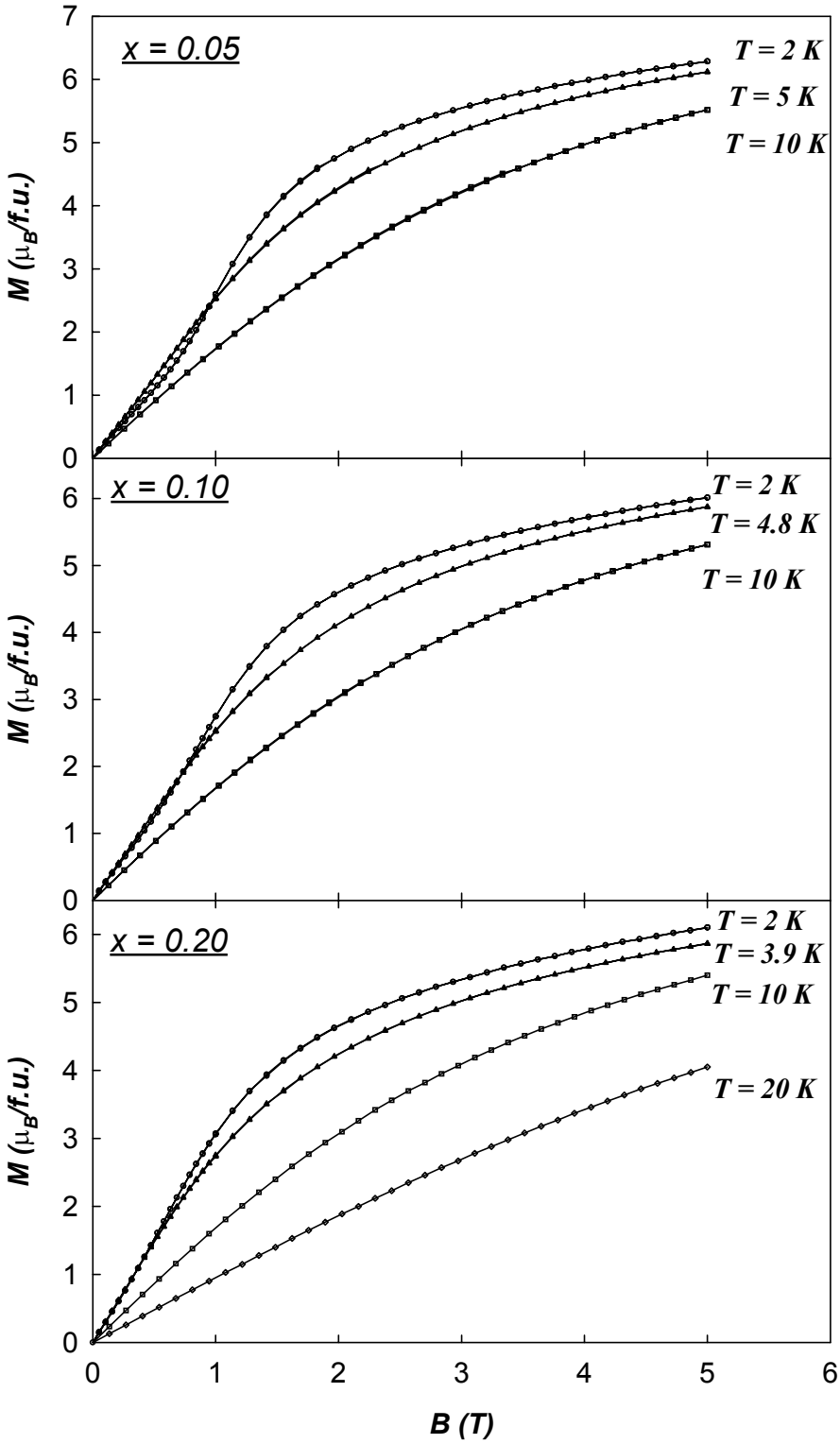

Fig. 5.14*: The magnetization curves of the samples with x = 0.05, 0.10 and 0.20 measured at different temperatures.*

5.3.3 0.40 ≤ x ≤ 0.80

The samples in this concentration region are characterized by a clear inflection point in temperature dependence of magnetization in contrast to that with low amount of Cu (see *Figs. 5.15* and *5.16*). The samples with 40% and 60% of the Cu-substitution exhibit one maximum in the low-temperature magnetization data. There are visible three maxima in the temperature dependence of the specific heat capacity of the 40%-Cu compound. We have obtained three values of phase transition corresponding to each of the observed anomalies. The highest one in the temperature, at about 5.1 K, corresponds to the inflection point of the magnetization (i.e. minimum of the first derivative in the *Fig. 5.15*). This point is probably the ordering temperature and we suppose the inflection point (T_{infl} = 4.3 K) in the sample with x = 0.60 to be ordering temperature too. The other one heat capacity anomaly, originating from a very weak anomaly, is at the temperature of 3.4 K. Such temperature corresponds to phase transition of erbium oxide (see also *Fig. 5.12* for x = 0.05).

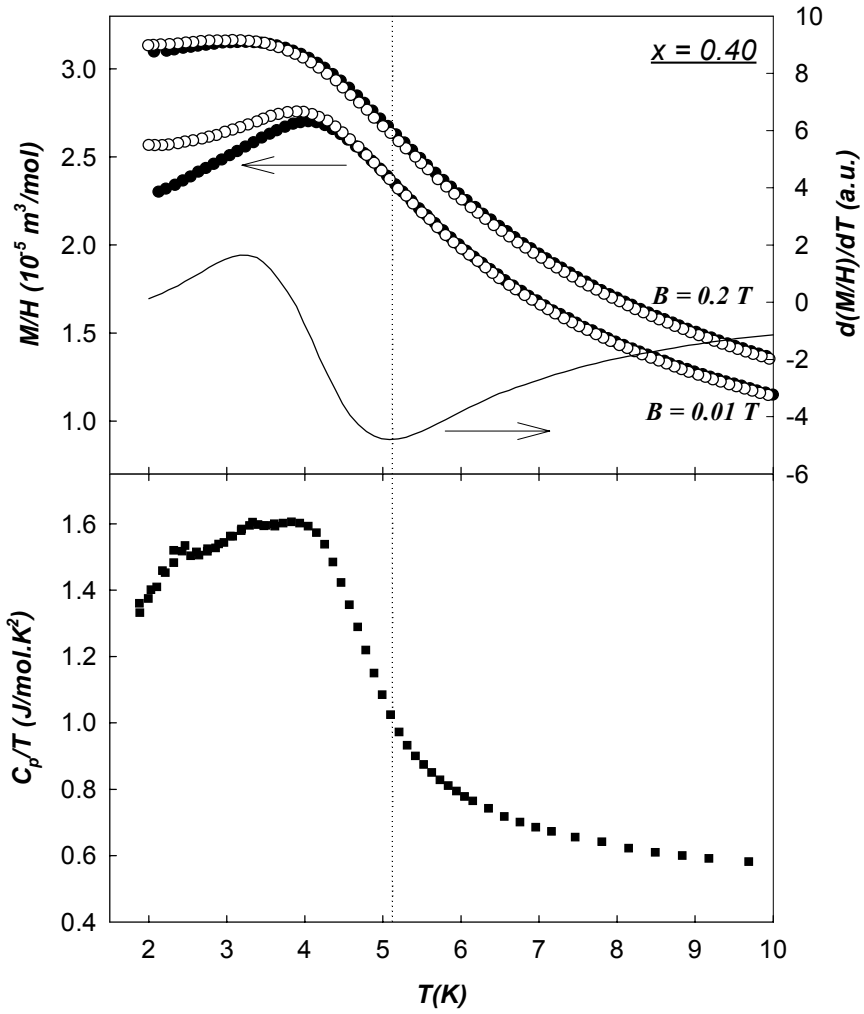

***Fig. 5.15**:*
The temperature dependence of M/H and C_p in the low temperature region for the $ErNi_{0.6}Cu_{0.4}Al$ compound.
The magnetization data have been measured in different magnetic fields with regime field-cooled (open symbols) and zero field-cooled (full symbols). The first derivative of field-cooled data at 0.01 T is represented by the solid line. The heat capacity have been measured without external field. The vertical dotted line represents the magnetic ordering temperature.

The last point (2.5 K) corresponding to the third, also weak maximum has no equivalent among important points of the magnetization dependence like extreme or inflection point. On the other hand, the maximum in magnetization dependence does not correspond to any anomaly in C_p data. It is questionable, if at these points phase transition appears.

The compound in the middle of the concentration area embodies no maximum in the field-cooled regime, just the inflection point at approximately 5.8 K. If magnetic ordering can be found in this compound, this temperature should be the ordering one like the sample with $x = 0.80$ (see *Fig. 5.16*). The ordering temperature of this compound is probably at the temperature of $T_{order} = 5.3$ K, which is derived from the zero value of the second derivative in the *M/H* vs. *T* dependence.

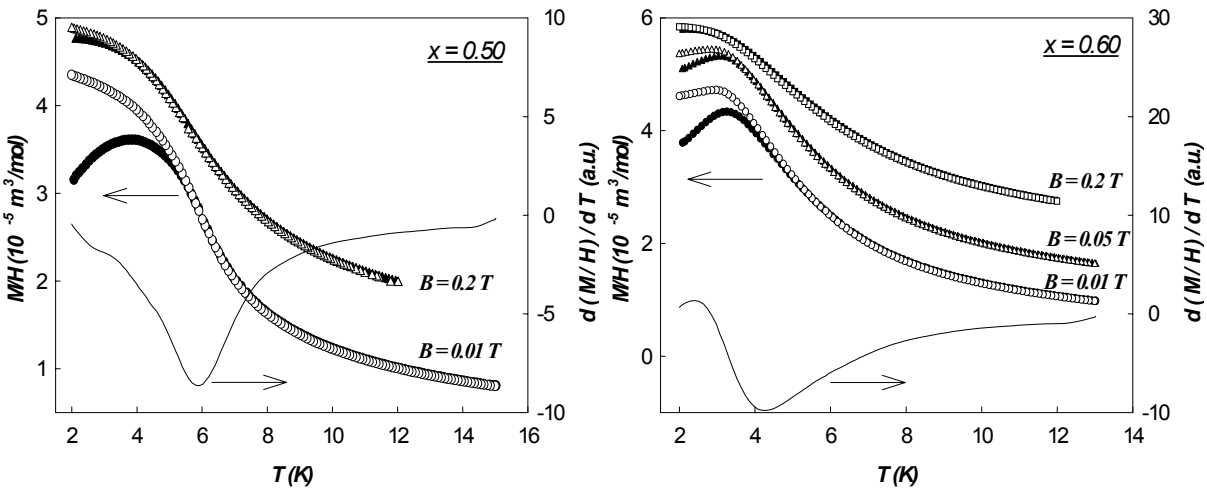

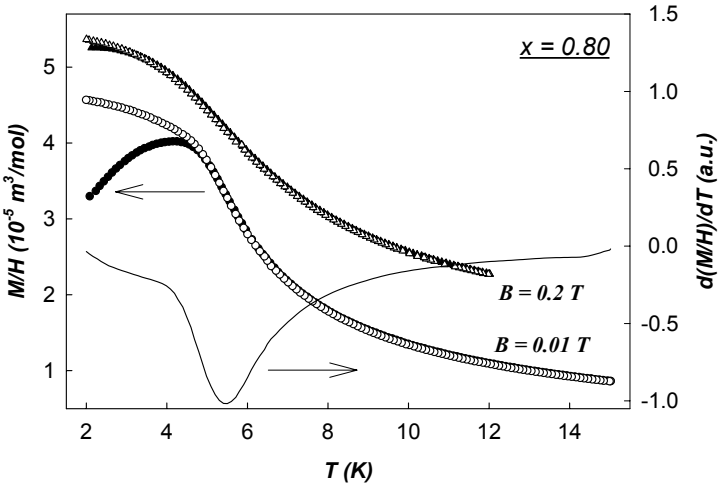

***Fig. 5.16**: The temperature dependence of M/H in the low temperature region for the $ErNi_{1-x}Cu_xAl$ samples with x = 0.50, 0.60 and 0.80 measured in different magnetic fields with regime field-cooled (open symbols) and zero field-cooled (full symbols).*

The magnetization curves contain already no double-curved behaviour as those for $x \leq 0.20$ (see *Fig. 5.17*). The magnetization curves of the compound with $x = 0.80$ do not exhibit the curvature with a rapid increase of magnetization just at low fields, typical for ferromagnetic compounds. But when we compare such curve with the similar one for the ErCuAl compound, there is no appreciable difference visible. The arrot plot for this compound in comparison to that of ErCuAl (*Fig. 5.18*) exhibits similar shape. Due to the reality that ErCuAl is surely ferromagnet according to the neutron scattering data (see section *3.3*), we propose $ErNi_{0.20}Cu_{0.80}Al$ to be a ferromagnet too.

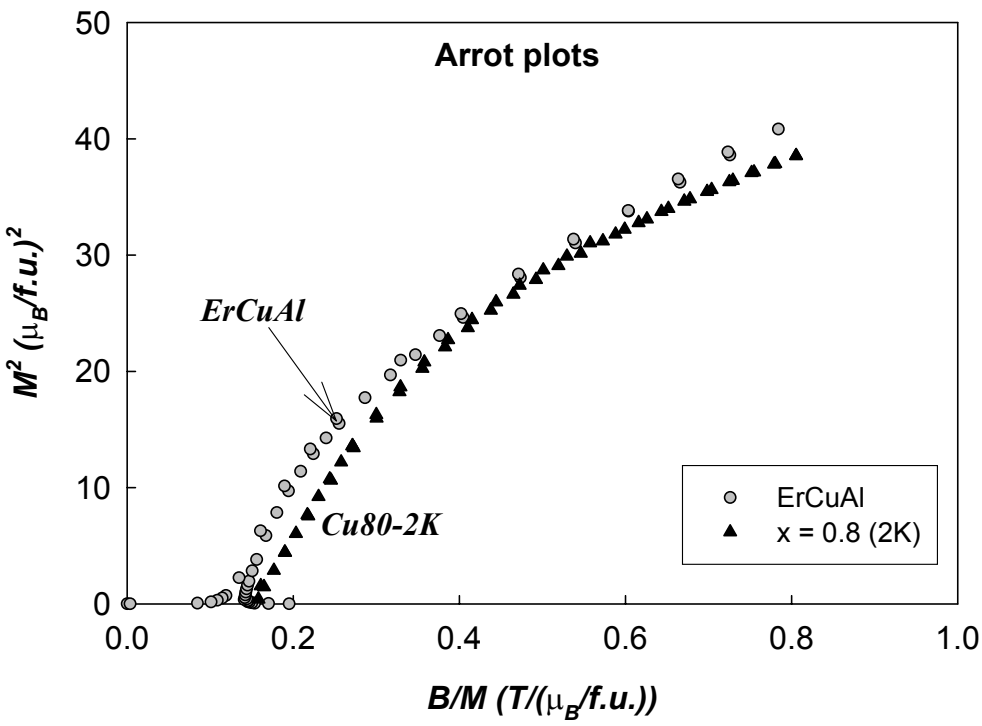

Fig. 5.18*: The Arrot plots for the $ErNi_{0.20}Cu_{0.80}Al$ and ErCuAl compounds at the temperature of 2 K.*

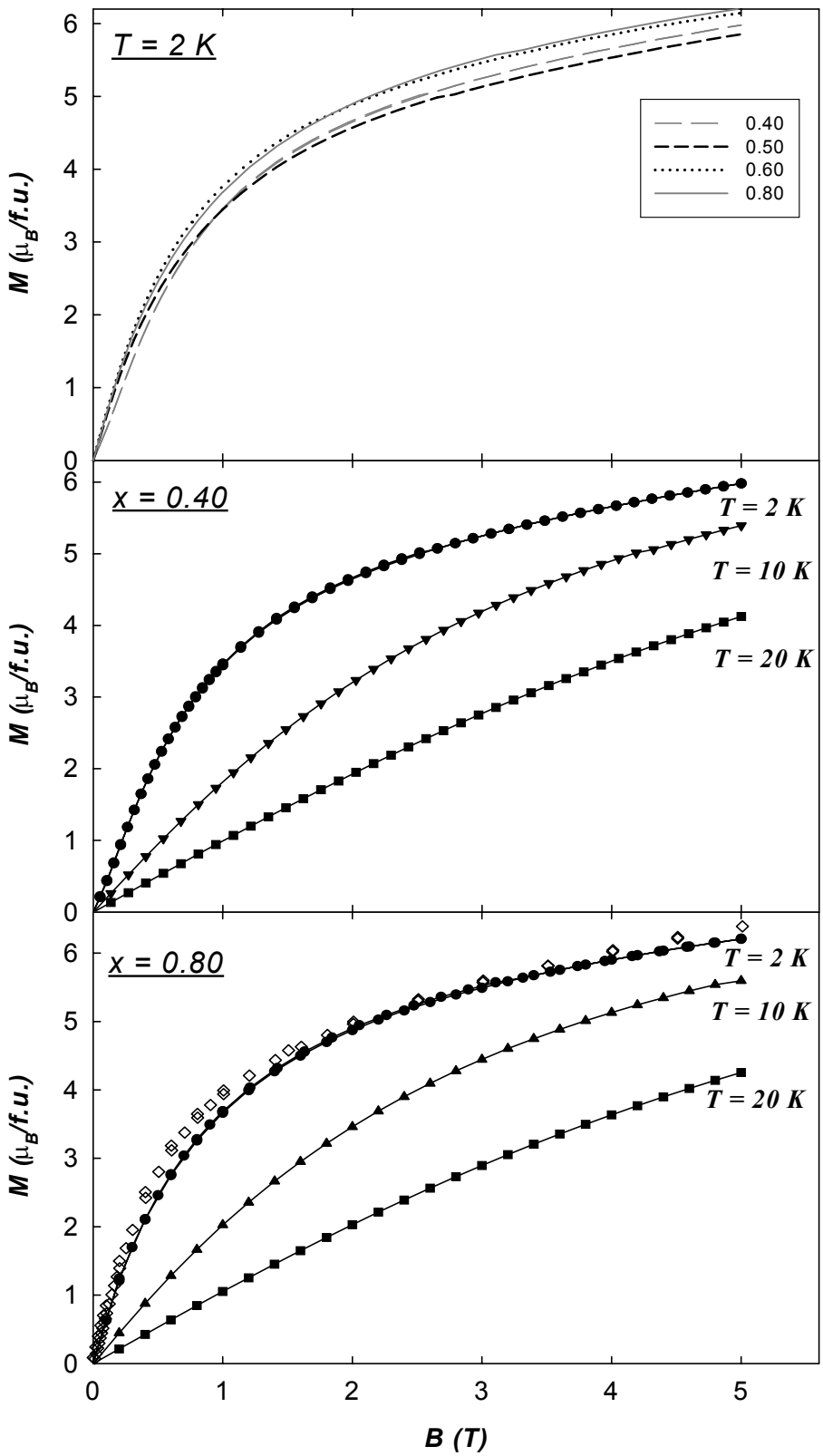

Fig. 5.17: *The magnetization curves of $ErNi_{1-x}Cu_xAl$ compounds with $0.40 \leq x \leq 0.80$ measured at 2 K (the upper graph) and for the compounds with x = 0.40 and 0.80 at different temperatures. For comparison, the magnetization curve of ErCuAl at 2 K is added (the last graph), being represented by empty diamonds.*

5.3.4 $ErNi_{0.9}Co_{0.1}Al$

The low-temperature dependences of M/H in the $ErNi_{0.9}Co_{0.1}Al$ sample exhibit a clear maxima up to the external fields of 0.2 T (*Fig. 5.19*). This indicates

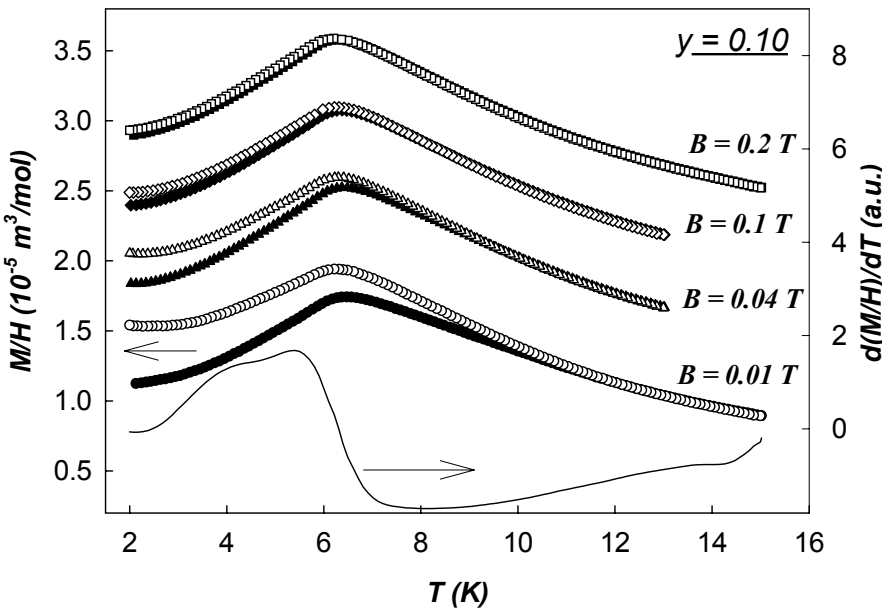

***Fig. 5.19**: The temperature dependence of M/H in the low temperature region for the $ErNi_{0.9}Co_{0.1}Al$ sample measured in different magnetic field with regime field cooled (open symbols) and zero-field cooled (full symbols). The data for stronger magnetic field are shifted to higher values (for better view).*

the phase transition to an antiferromagnetic order below the maximum. The maximum happens at 6.3 K and we can propose this temperature as the ordering temperature. The magnetization curve at 2 K indicates a magnetic phase transition from the antiferromagnetic ordering in fields lower than ~ 1 T most probably to a simple ferromagnetic order in higher fields (*Fig. 5.20*).

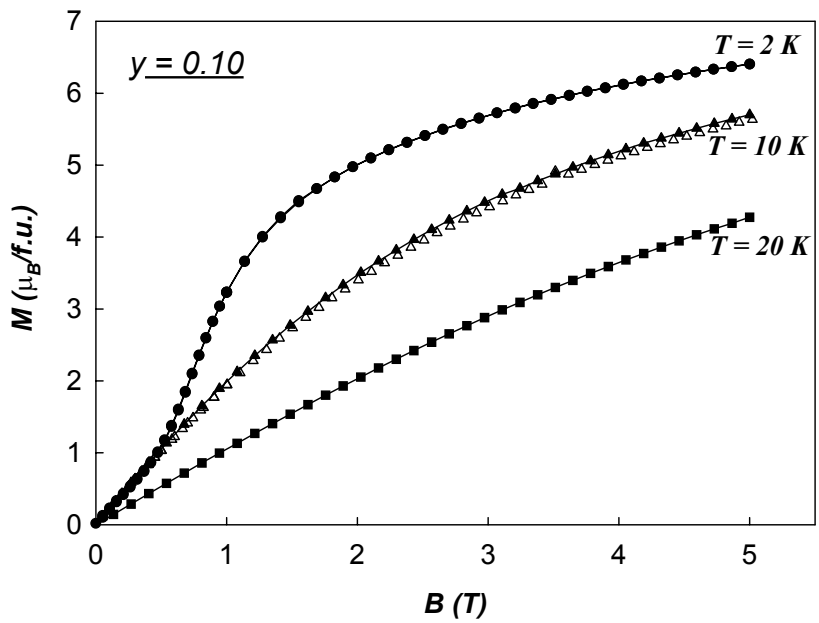

***Fig. 5.20:** The magnetization curves of $ErNi_{0.9}Co_{0.1}Al$ measured at different temperatures (full symbols ~ PPMS, open symbols ~ SQUID).*

Table 5.5a: *The summary of the maxima and inflection points of the $ErNi_{1-x}Cu_xAl$ and $ErNi_{0.9}Co_{0.1}Al$ compounds derived from the magnetization data at 0.01 T in the field-cooled regime. The only exceptions are the x = 0.10 and 0.20(Cu) samples. For them the zero field-cooled (zfc) data have been used.*

x	T_{infl} (K)	T_{max1} (K)	T_{max2} (K)
0.05 (zfc)	—	5.5 ± 0.2	4.5 ± 0.2
0.10 (zfc)	—	4.9 ± 0.2	4.4 ± 0.2
0.20	?	4.3 ± 0.2	3.1 ± 0.3
0.40	5.1 ± 0.2	3.9 ± 0.2	—
0.50	5.8 ± 0.2	—	—
0.60	4.3 ± 0.2	2.9 ± 0.3	—
0.80	5.3 ± 0.2	—	—
0.10 (Co)	—	6.3 ± 0.2	—

Table 5.5b: *The anomaly points derived from the heat capacity data measured at the zero external field for $ErNi_{0.95}Cu_{0.05}Al$ and $ErNi_{0.60}Cu_{0.40}Al$ compounds.*

x	T_{order} (K)	T_1 (K)
0.05 C_p	5.7 ± 0.2	4.4 ± 0.2
0.40 C_p	5.1 ± 0.2	2.5 ± 0.1

6. Summary and discussion

From the different alignment of magnetic moments in ErNiAl and ErCuAl compounds, the change of magnetocrystalline anisotropy and the transition from antiferro- to ferromagnetic order within the pseudo-ternary series $ErNi_{1-x}Cu_xAl$ is expected.

Viewing the concentration dependence of lattice constants, we observe a sudden 'jump' in the interval $0.50 \leq x \leq 0.60$, that separates the whole series into 2 sections. This strong shift probably holds also in the low temperatures down to at least 5 K, as it can be deduced from the data of compounds with $x = 0.00$; 0.40; 0.50 and 1.00. For the concentration dependence at T = 50 or 5 K, respectively, we do not have as many points as for the room temperature, but *a* and *c* do not follow monotonic increase as in the Tb-based series. A small increase of the *a*- and *c*-parameters within each of these sections separately is reasonable and it may originate in the difference of Ni- and Cu-atomic radii. A question then arises, whether the sudden jump of *c*/*a* ratio is connected with a change of the direction of magnetic moments and/or with the change of the type of magnetic order. Magnetization data clarify this question only partly.

In the concentration range $0.05 \leq x \leq 0.20$ low-temperature magnetization embody two maxima. For the 5% sample, their positions agree well with anomaly points in the heat capacity data, so we can consider them to be the phase transition temperatures. Although the heat capacity has not been measured on two out of these samples ($x = 0.10$; 0.20) at time of the end of this thesis yet, we expect the same correspondence also for the other "two-maxima" compounds, i.e. $x = 0.10$ and 0.20, and we propose these maxima to be points of the phase transition. Certainly, it will be useful to measure heat capacity on these samples in the future. The shape of magnetization curves at 2 K indicates presence of AF order, at least an antiferromagnetic component. This feature is evident for the 5% and 10% samples, it becomes less clear with increasing the Cu-content, and is almost lost for the 20% compound. The 20% Cu-substituted compound exhibits already sign of the inflection point in the M/H vs. T dependence, which becomes clearly visible in magnetization data of samples with higher amount of copper ($x \geq 0.40$). It may indicate the rising ferromagnetic ordering. In the concentration region of $x \leq 0.20$ the coexistence of ferro- and antiferromagnetically ordered components is possible, while the ferromagnetic one becomes stronger with increasing parameter *x*. A neutron diffraction experiment is needed to describe the magnetic ordering in detail.

The low-temperature magnetization dependencies of the other samples ($0.40 \leq x \leq 0.80$) exhibit a clear inflection point. For the 40%-Cu compound

the inflection point in magnetization data at 5.1 K indicates the second order-type phase transition to magnetically ordered state. The shape of the anomaly in the heat capacity corresponds to this thesis and we suppose this accordance to be held in all the other compounds exhibiting similar behaviour with the inflection point that indicates most likely the ferromagnetic ordering, although this should be confirmed by heat capacity in the future. The samples with x = 0.40 and 0.60 embody the maximum in magnetization dependencies. As it doesn't correspond, for 40% sample, to any important point of the specific heat data (accordance with its maximum has probably no physical meaning), we are not sure about its origin or if these maxima are connected with any magnetic effect.

Although the magnetization curves of the $ErNi_{0.60-0.20}Cu_{0.40-0.80}Al$ compounds do not exhibit typical ferromagnetic behaviour, we tend to a conclusion, that they are ferromagnets, because of the similarity with the ErCuAl compound. It has a similar shape of the magnetization curve (*Fig. 5.17*), and has been confirmed as ferromagnet by means of neutron diffraction [1].

The data of heat capacity for both the samples $x = 0.05$ and 0.40 embody weak anomaly at about 3.4 K. This maybe caused by the presence of erbium oxide, which exhibit the anomaly at this temperature. The erbium oxide was not detectable by the microprobe experiment at the conditions as used, but we cannot exclude small amount of it as well as its formation on the surface of sample used for specific heat measurements.

The above mentioned indicates, that the transition from antiferro- (AF) to ferromagnetic (F) ordering happens rather gradually with increasing parameter x and it is not connected with the structure change. Type of the ordering is therefore influenced by one electron, which is being added into the configuration of the transition metal by substituting Cu ([Ar] $3d^9\ 4s^2$) instead of Ni ([Ar] $3d^8\ 4s^2$). We do not observe any indications for disappearing of long-range magnetic order, unlike the $TbNi_{1-x}Cu_xAl$ series, where it is almost lost in a rather large concentration region [3].

It is not clear yet, at which concentration x the change of anisotropy comes on and 1) if it is the consequence of the lattice transformation or 2) if it happens in connection with the AF to F transition through the concentration range. The structure 'jump' induces change of the crystal field, so the first theory would be more acceptable. In such case the compound with $x = 0.40$ (and 0.50 probably too) is the ferromagnet (magnetization data) with alignment of the moments within the basal plane. Magnetic ordering of this kind has not been observed in any *RTX* compound crystallizing in the ZrNiAl-type structure. Solution of this unclearness is the question for neutron scattering experiments.

The only sample with the Co-substitution has been studied by means of magnetization. The obtained data show typical antiferromagnetic dependencies, so we can say it is likely an antiferromagnet. The second sample from the $ErNi_{1-y}Co_yAl$ series that we have prepared (with $y = 0.2$) contained considerably some more impurity phases as revealed by x-ray diffraction pattern. As the ErCoAl compound does not crystallize in the ZrNiAl-type crystal structure, already 20% of Co-substitution may inject some other phases with different structure type, which can influence the bulk properties. Thus we haven't done any of the magnetic measurements on this sample.

7. Conclusions

We have studied the pseudo-ternary compounds $ErNi_{1-x}Cu_xAl$ and part of the $ErNi_{1-y}Co_yAl$ ($y = 0.1$ and 0.2) series from the view of the crystal structure and magnetic properties. The quality of the samples has been investigated by x-ray and microprobe experiments. The magnetic study is based mainly on magnetization measurements and for two samples ($x = 0.05$ and 0.40) also on specific heat data.

All the studied compounds crystallize in the ZrNiAl-type hexagonal structure, but in the $ErNi_{0.8}Co_{0.2}Al$ sample already large amount of impurity phases appears. Higher Co-substitution rate induces the transition to different type of crystal structure. The series $ErNi_{1-x}Cu_xAl$ exhibit a clear lattice "jump" in the middle concentration region ($0.5 \leq x \leq 0.6$) at the room temperature. This sharp change of the structure is probably retained also at low temperatures down to at least 5 K. It is the question if this effect is connected with the change of magnetocrystalline anizotropy.

The compounds in the concentration range from $x = 0.05$ to 0.20 exhibit at least two phase transitions. For the sample with $x = 0.05$ this fact is confirmed by the data from measurig of the heat capacity. The maxima indicating probably antiferromagnetic ordering move to lower temperatures with increasing parameter x. The coexistence of ferro- and antiferromagnetic components is not precluded with a gradual strengthening of the F component with increasing Cu concentration. The compounds with $x \geq 0.40$ exhibit behaviour more similar to the boundary compound, ErCuAl, which is surely ferromagnet. Thus we tentatively conclude to a F order in these compounds, although a more complex ordering cannot be excluded especially for 0.40 to 0.60 concentrations.

It means that the change from antiferro- to ferromagnetic type of order is not connected with the sudden jump of lattice parameters. It is more likely related to the gradual filling of the 3*d*-band of the transition metal as increasing Cu-concentration. Whether the change of magnetocrystalline anisotropy is related to the structural change is not clear at the moment.

One sample with the substituted Co elements instead of Ni has been studied by magnetization measurements. It exhibits typical antiferromagnetic dependencies.

To clear the type and direction of the magnetic ordering within the $ErNi_{1-x}Cu_xAl$ series we propose further study of these compounds, especially the neutron diffraction experiment. The determination of the orientation of magnetic moments can help to our better understanding of the relation between the crystal and magnetic structure.

8. References

[1] P. Javorský: Magnetism in *R*CuAl and *R*NiAl compounds, doctoral thesis, 1997

[2] N. C. Tuan: Magnetism in *R*NiAl compounds, Thesis, Prague, 1992

[3] G. Ehlers, D. Ahlert, C. Ritter, W. Miekeley, H. Maletta; *Europhysics Letters,* **37(4)** (1997) 269-274

[4] Ch. Kittel: *Úvod do fyziky pevných látek,* Academia, Praha, 1985

[5] M. T. Hutchings, *Solid State Phys.* **16** (1964) 227

[6] H. A. Kramers: *Koniki. Ned. Akad. Wetenschap., Proc.* B33 (1930) 959

[7] H. A. Jahn and E. Teller: *Proc. Roy. Soc.* **A161** (1937) 220

[8] N. W. Ashcroft, N. D. Mermin: *Solid State Physics,* Saunders College, Philadelphia, 1976

[9] I. A. Campbell, *J. Phys. F: Metal Phys.* **2** (1972) L47

[10] V. Sechovský, L. Havela, in E. P. Wohlfahrt, K. H. J. Buschow (eds.): *Ferromagnetic materials*, **vol. 4**, North-Holland (1988) p. 309

[11] A. Szytuła, M. Kolenda, J. Leciejewicz, N. Stüsser: *J. Magn. Magn. Mat.* **164** (1996) 377

[12] Ch. D. Routsi, J. K. Yakinthos, E. Gamari-Seale: *J. Magn. Magn. Mat.* **110** (1992) 317

[13] A. Szytuła, B. Penc, M. Kolenda, J. Leciewicz, N. Stüsser, A. Zygmunt: *J. Magn. Magn. Mat.* **153** (1996) 273

[14] B. Gibson, R. Pöttgen, R. K. Kremer, A. Simon, K. R. A. Ziebeck: *J. Alloys and Compounds* **239** (1996) 34

[15] K. C. Watson, J. Crangle, K. U. Neumann, K. R. A. Ziebeck: *J. Magn. Magn. Mat.* **140-144** (1995) 883

[16] F. Hulliger: *J. Alloys and Compounds* **218** (1995) 44

[17] H. Fujii, M. Nagasawa, H. Kawanaka, T. Inoue, T. Takabatake: *Physica B* **165&166** (1990) 435

[18] H. Kitazawa, A. Matsushita, T. Matsumoto, T. Suzuki: *Physica B* **199&200** (1994) 28

[19] J. Diehl, H. Davideit, S. Klimm, U. Tegel, C. Geibel, F. Steglich, S. Horn: *Physica B* **206&207** (1995) 344

[20] C. Schank, G. Olesch, J. Köhler, U. Tegel, U. Klinger, J. Diehl, S. Klimm, G. Sparn, S. Horn, C. Geibel, F. Steglich: *J. Magn. Magn. Mat.* **140-144** (1995) 1237

[21] T. Fujita, K. Satoh, Y. Maeno, Y. Uwatoko, H. Fujii: *J. Magn. Magn. Mat.***76&77** (1988) 133

[22] H. Fujii, T. Inoue, Y. Andoh, T. Takabatake, K. Satoh, Y. Maeno, T. Fujita, J. Sakurai, Y. Yamaguchi: *Phys. Rev. B* **39** (1989) 6840

[23] A. E. Dwight, Muller, Conner Jr., Downey, Knott: *Trans. Met. Soc. AIME* **242** (1968) 2075

[24] H. Oesterreicher: *J.Less-Common Metals* **30** (1973) 225

[25] G. Ehlers, H. Maletta: *Z. Phys. B* **101** (1996) 317

[26] P. Javorský, P. Burlet, V. Sechovský, R. R. Arons, E. Ressouche, G. Lapertot: *Physica B* **234-236** (1997) 665

[27] P. Javorský, V. Sechovský, R. R. Arons, P. Burlet, E. Ressouche, P. Svoboda and G. Lapertot: *J. Magn. Magn. Mat.* **164** (1996) 183

[28] P. Javorský, L. Havela, V. Sechovský, H. Michor, K. Jurek: *J. Alloys and Compounds* **264** (1998) 38

[29] P. C. M. Gubbens, R. van Geemert, K.H.J. Buschow: *J. Magn. Magn. Mat.* **177-181** (1998) 1149

[30] P. Javorský et al., to be published

[31] P. Javorský, P. Burlet, E. Ressouche, V. Sechovský, H. Michor, G. Lapertot; *Physica B* **225** (1996) 230-236

[32] P. Javorský, M. Diviš, H. Sugawara, H. Sato, H. Mutka: *Physical Review B*, **65** (1) 014404 (2002)

[33] G. Ehlers, H. Maletta: *Z. Phys B* **99** (1996) 145

[34] Program Fullprof, Laboratoire Léon Brillouin,T. Roisnel, http://www-llb.cea.fr/fullweb/winplotr/winplotr.htm

[35] V. Hulinský, K. Jurek: *Zkoumání látek elektronovým svazkem,* SNTL Prague 1983

[36] Kevex manual

[37] PPMS manual